공학석사학위논문

분산발전용 용융탄산염 연료전지와 HCCI 엔진의 하이브리드 시스템 최적화

Optimization of Molten Carbonate Fuel Cell (MCFC) and Homogeneous Charge Compression Ignition (HCCI) Engine Hybrid System for Distributed Power Generation

2013 년 8 월

서울대학교 대학원

기계항공공학부

김 선 엽

분산발전용 용융탄산염 연료전지와 HCCI 엔진의 하이브리드 시스템 최적화

Optimization of Molten Carbonate Fuel Cell (MCFC) and Homogeneous Charge Compression Ignition (HCCI) Engine Hybrid System for Distributed Power Generation

지도교수 송 한 호

이 논문을 공학석사 학위논문으로 제출함

2013 년 8 월

서울대학교 대학원
기계항공공학부
김 선 엽

김선엽의 공학석사 학위논문을 인준함

2013 년 8 월

위 원 장 민 경 덕 (인)

부위원장 송 한 호 (인)

위 원 김 찬 중 (인)

Abstract

Optimization of Molten Carbonate Fuel Cell (MCFC) and Homogeneous Charge Compression Ignition (HCCI) Engine Hybrid System for Distributed Power Generation

Seonyeob Kim

School of Mechanical and Aerospace Engineering

The Graduate School

Seoul National University

The demand for renewable power sources rises due to environmental issues and resource depletion. Fuel cell system is concerned as one of the alternatives. A new MCFC-HCCI engine hybrid system model, which is combined of a fuel cell and an internal combustion engine, had been developed previously by the author. The engine was added to the hybrid

system instead of a catalytic burner in standalone system. The hybrid system efficiency increased to about 62%. However, the engine size is too large in comparison with general engine, which yields same power output. Therefore, the engine is ineffective for cost. Firstly, in this study, the system was optimized by downsizing the engine for reduction the cost. There were several strategies for downsizing the engine, e.g. using a turbocharger, increasing a compression ratio of the engine. For using these methods, we could suggest the optimized hybrid system. The engine of the optimized system was downsized over 60%. Secondly, an approach to broaden the operating range was studied by running under various strategies which enables flexible power output, e.g. 70-100% power ratio. As a result, we analyzed the performance of the system and confirmed that this is feasible for off-design operation.

Keywords: MCFC, HCCI engine, Turbocharger, Hybrid system, Optimization, Off-design operation

Student Number: 2011-23328

List of Tables

List of Figures

Nomenclature

A_{seg}	area of each segment (cm^2)
CI	compression ignition
ΔF	change in molar flow rate ($mol \cdot h^{-1}$)
ΔG	gibbs free energy change ($J \cdot mol^{-1}$)
ΔH	apparent activation energy for resistance parameters ($J \cdot mol^{-1}$)
E_{rev}	maximum reversible potential (V)
f	faraday's constant (96487 $C \cdot mol^{-1}$)
F	molar flow rate ($mol \cdot h^{-1}$)
H	frequency factor for resistance
F	parameters ($J \cdot mol^{-1}$)
i	current (A)
j	current density ($A \cdot cm^{-2}$)
K_p	equilibrium constant
M	molar fraction
NO_x	oxides of nitrogen
$ODEs$	ordinary differential equations
P	partial pressure (bar)
Q	energy required (J)
R	universal gas constant ($J \cdot mol^{-1} \cdot K^{-1}$)
R_{and}	irreversible loss at anode ($\Omega \cdot cm^{-2}$)
R_{cat}	irreversible loss at cathode ($\Omega \cdot cm^{-2}$)
R_{int}	internal cell resistance ($\Omega \cdot cm^{-2}$)
R_{total}	total irreversible loss ($\Omega \cdot cm^{-2}$)
r	specific heat ratio
T	temperature (K)
V_{opn}	operating cell voltage(V)
W	work output (J)
X	conversion degree

Greek Letter

η	loss

Subscripts

and	anode
and,i	species at anode
cat	cathode
cat,i	species at cathode
CO	carbon monoxide
CO_2	carbon dioxide
H_2	hydrogen molecule
H_2O	water
i	species
Nern	Nernst
X	Gas
c	compressor
t	turbine
comb	combustion

1. Introduction

1.1. Research background

Nowadays, the interest in renewable energies rises due to environmental concerns and resource depletions. Fuel cell technology is considered as a promising candidate for this category with its high efficiency and almost zero pollutant emission. Among various types of fuel cell, fuel cells operating at high temperature generally show higher efficiency than those operating at relatively lower temperature [1]. There are two major types of high-temperature fuel cells, which are solid oxide fuel cell (SOFC) and molten carbonate fuel cell (MCFC). The former is still under active research and development stage, but the latter is already commercialized for distributed power generation purpose.

1.2. Previous researches

Several studies have attempted to hybridize these high-temperature fuel cell systems with other power generating technology, in order to achieve the additional power and to improve the efficiency of the overall system. Due to its operating characteristics of MCFC, there have been many efforts to build the hybrid system on it. The hybrid system, which is

MCFC coupled with gas turbine, is studied by several researches [2-7]. Lunghi et al. analyzed the hybrid MCFC gas turbines system, and optimized the hybrid system. In that study, it is possible to increase to over 58% efficiency of the hybrid system by a parametric performance evaluation [2]. Roberts et al. show a dynamic simulation of MCFC/GT hybrid system. The hybrid system efficiency is under 57% [3]. Ubertini et al. show MCFC system with a steam injected gas turbine. The system overall electrical efficiency is 69% [4]. Liu et al. presents a hybrid system composed of a pressurized MCFC and a micro GT. They designed the hybrid system, and analyzed the system at off-design operation. The system efficiency is about 58% [5]. Rashidi et al. show a combined MCFC system including a turbo expander. The system efficiency is about 60% [6]. Orecchini et al. proposed MCFC and microturbine system model. They developed MCFC model, plate reformer model and micro turbine-compressor model. The hybrid system electrical efficiency is about 74% [7]. For heat recovery, MCFC system with organic Rankin cycle (ORC) is researched [8-10]. Angelino et al. research organic Rankine cycles for heat recovery. They simulate a MCFC plant with ORCs using different fluids. The system efficiency is under 60% [8]. Sanchez et al. introduce a hybrid system, which is composed of MCFC, gas turbine and ORC. They optimized the system, and the hybrid system net efficiency is under 59% [9]. Recently, Vatani et al. study heat recovery from direct

internal reforming MCFC (DIR-MCFC). They analyzed the system which is composed of ORC and a DIR-MCFC. The system efficiency is about 60% [10]. For high efficiency, hybrid system which is composed of MCFC and Stirling engine is studied [11, 12]. Sanchez et al. show a new design for hybrid system, which is composed of Stirling engine and MCFC. They compared the hybrid system with MCFC-Rankine system and MCFC-Brayton system. The MCFC-Stirling system efficiency is about 61%, which is higher than the efficiency of the other systems [11]. Recently, Escalona et al. analyzed two hybrid systems, which are MCFC-Stirling system and MCFC-SCO2 (supercritical carbon dioxide turbines) system. The MCFC-Stirling system efficiency is 56% and the MCFC-SCO2 system efficiency is about 59% [12]. Although many hybrid systems was introduced, most researches are focused on large-scale power generation, except for MCFC-Stirling system.

Recently, we developed a new MCFC-HCCI engine hybrid system for sub-megawatts distributed power generation [13]. This new hybrid system was modeled by using the Mathworks Matlab and Cantera toolbox, and compared with the standalone counterpart. At comparable boundary conditions, the former demonstrated ~20% (relative) improvement in both power output and system efficiency, as compared to the latter, which proved itself to be a promising candidate for highly-efficient distributed power generation system in the near future.

Figure 1.1 shows a schematic of systems, which is developed by the authors. Figure 1.1 (a) shows standalone system using catalytic burner, and (b) shows hybrid system adopting HCCI engine. The system inlet gas (state 1), which is methane mixed with water in a mole ratio of 1:2.5, is preheated by HX5, HX1 for satisfying the fuel cell operating temperature. After reacting in the MCFC, anode off-gas (state 5) enters radiator and condense out partial water vapor for downsizing the engine size. The anode off-gas (state 6), which is mixed with air (state st) in MIX1, is preheated by HX4, and then enters the burner or HCCI engine. After combusting in burner or HCCI engine, the exhaust gas (state9) enters the cathode by being mixed with air, which is preheated by anode off-gas and cathode off-gas.

1.3. Research subjects

In this paper, we present the results from our continuing efforts to demonstrate the feasibility of the hybrid system in a real-world application. There were three major issues discussed in our previous work [13]:

1. Engine size and its associated cost
2. Power variation or off-design operation
3. Start-up or shut-down strategies

We are focusing on the first two topics in this paper, and the third topic is discussed in our companion work [14], since it requires quite extensive modeling efforts and discussions by itself.

In the first topic, our goal is to downsize the engine and thus increase the specific power output. Our previous system adopted an 18.4-liter HCCI engine for 300 kW MCFC system. The engine output at design point operation was about 55.3 kW. It is noted that the typical power output in that size of the engine is ~10 times higher, or ~500 kW, which implies that the engine size in the original design was not at all optimized and may cause significant amount of extra cost that might be avoided otherwise. Therefore, downsizing the engine will lead to the cost reduction of the hybrid system, which, in the end, improves the feasibility of it.

The engine size is directly correlated with the required volume flow rate of the intake flow, in order to avoid creating the vacuum pressure in the system, if the engine tries to intake more volume than the fuel cell supplies, or generating back-pressure, if the engine can't take the volume flow rate from the fuel cell. Thus, to downsize the engine, the volume flow rate from the fuel cell to the engine should be decreased. The following options can be considered: 1. mass flow rate reduction from the fuel cell to the engine, 2. lower intake temperature, and 3. higher intake pressure.[1)] The engine intake charge consists of the anode off-gas from

the MCFC and the fresh air as an oxidizer for the engine operation. Here, the anode off-gas is composed of CO, CO2, H2 and H2O. Among these species, H2O is relatively easy to be removed by condensation to reduce the mass flow rate to the engine. In our original system, the water-condensing radiator for the anode-off gas was already adopted. In this study, to achieve the lower intake temperature and higher intake pressure, the use of higher geometric compression ratio and turbocharger are considered, respectively.

For the second topic of power variation, it is noted that the fuel cell hybrid system should be able to run at various power levels, although it is generally operated at a constant or designed power output level. Due to the complication of the additional degree-of-freedom by having the engine in the hybrid system, new power variation strategies need to be developed.

The main body of this paper are comprised of three sections, i.e. Modeling Descriptions, Engine Downsizing, and Off-design Operation. In Modeling Descriptions section (Section 2), detailed modeling descriptions on the major components, such as MCFC stack or HCCI engine, and the system integration are provided. In Engine Downsizing section (Section 3), the aforementioned techniques for downsizing the engine, i.e. use of high geometric compression ratio and turbocharger, are discussed. Finally, in

1) The engine speed can be increased to intake higher volume rate in a given engine size, but in our study, we fix the speed at 1800 RPM, which is a typical number for the engine sizes that we consider.

Off-design Operation section (Section 4), the newly-developed system with downsized engine from Section 3 is used to develop the operating strategies of the hybrid system at various power levels. The system performance at off-design operation will also be shown.

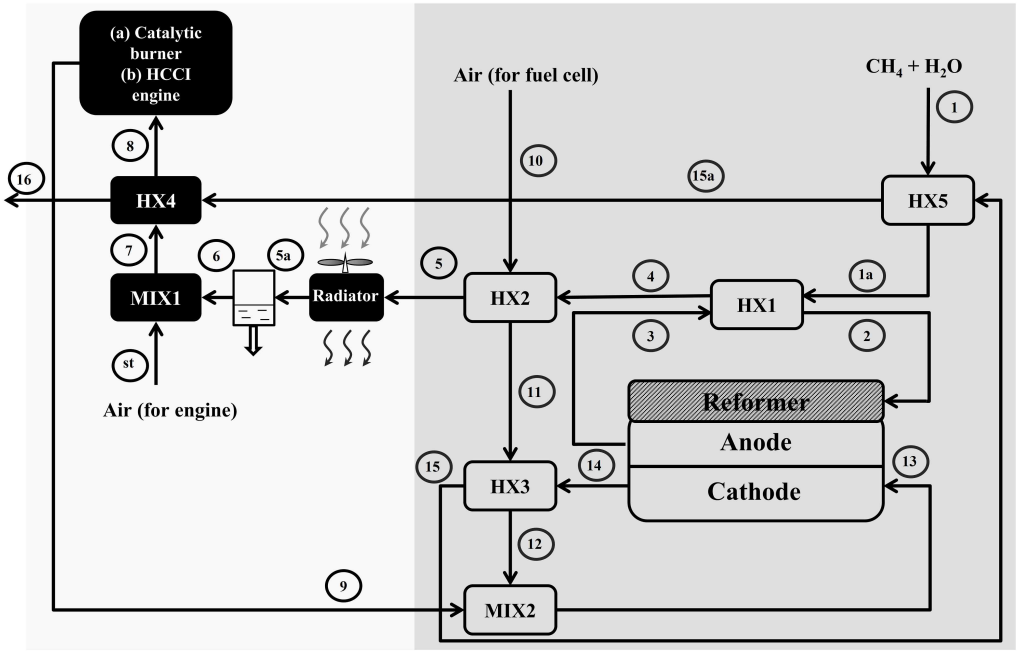

Figure 1.1 (a) Standalone system (with catalytic burner) (b) Hybrid system (with HCCI engine)

2. Modeling Descriptions

In this section, detailed modeling descriptions about the components of the hybrid system are discussed. The hybrid system is composed of MCFC stack, HCCI engine, heat exchanger, mixer and turbocharger. To analyze the hybrid system performance, component modeling was executed by using the Mathworks MATLAB and Cantera toolbox which is computing thermochemistry reactions. The models are previously developed by author except turbocharger model, so the model description will be described briefly in this section. Firstly, hybrid system configuration is discussed. The system model is developed previous study, and the model is described for the gas flows in this section. Secondly, MCFC stack model is described. The model, which is one-dimensional and non-isothermal, is described for gas flow, various loss and temperature change in the fuel cell. Thirdly, HCCI engine model is discussed. The engine model, which is zero-dimensional, is described for engine specifications and operating conditions. Finally, turbocharger model, which is developed newly in this paper, is discussed. The model specification and modeling process are mentioned.

2.1. Hybrid system

Figure 2.1 shows a hybrid system configuration, which is added to a turbocharger in comparison with the system developed previously. Gas

flow in the system is similar to most gas flow described in section 1, but some states affix to the system due to addition of the turbocharger. The followings are descriptions about additional states and more explanation about the hybrid system.

The engine fuel-air mixture (state 6a) enters the compressor. The compressed mixture passing through the compressor (state 7) enters the engine. The engine exhaust gas (state 8a) comes in the turbine. After expanding, the atmosphere pressure gas (state 9) enters the mixer for supplying the mixture to cathode side (state 13).

Methane (CH4) with steam (H2O) (state 1) enters heat exchanger (HX5) before entering reformer of MCFC. S/C ratio, which is mass flow rate of steam over mass flow rate of methane, is 2.5:1. HX5 acts as exchanging heat of system inlet gas (state 1) and cathode off-gas (state 15). System inlet gas (state 1) which is preheated by HX5 is heated one more by HX1 for satisfying MCFC operating temperature. Air for MCFC operation (state 10) is preheated by HX2 and HX3, which exchange heat of anode off-gas (state 4) and cathode off-gas (state 14) separately. After preheating, the air is mixed with engine exhaust gas (state 9) in mixer MIX2, and then enters cathode of MCFC. Anode off-gas (state 5) enters radiator and condense out partial water vapor for downsizing the engine size. It helps that the engine cost decreases. The gas (state 6) is mixed with air (state st) in MIX1. The engine fuel-air mixture (state 6a) enters

the compressor, and then preheated by HX4. At this time, cooled cathode off-gas (state 16) by HX4 exits the system. The compressed mixture (state 7) enters the engine. After combusting, the engine exhaust gas (state 8a) comes in the turbine. After expanding, the atmosphere pressure gas (state 9) enters the mixer for supplying the mixture to cathode side (state 13). In the system, the effectiveness of all heat exchanger in the system is lower than 85%.

2.2. MCFC stack modeling

MCFC stack model was developed for analyzing performance of the fuel cell in hybrid system. And this fuel cell model is developed in past study of authors [13] and the followings reference a master's thesis of Abid [15]. The present model takes a similar approach as described in Ref. [16] by Baranak et al., although their model is isothermal. The model assumptions are:

- Cathode and anode streams flow in parallel and assume the same temperature changes along the channels.
- Pressure change across the fuel cell channel is negligible.
- In reforming channel, the fuel mixture is fully reformed and achieves thermodynamic equilibrium at the exit, before it enters the anode channel.
- The water-gas-shift-reaction at anode channel occurs fast enough

to keep anode compositions at equilibrium all the time.

- Overall system operates under steady state condition.
- Natural gas, a fuel for typical MCFC system, is modeled as pure methane.

There are various reactions in fuel cell. Firstly, methane-steam mixture enters the reforming channel in fuel cell, and then the mixture changes H2, CO2, CO, and H2O by water-gas-shift-reaction (WGSR). The gas after reforming enters the anode channel and O2 and CO2 enter the cathode channel. O2 and CO2 change to CO32-, and then the carbonate ion transfers from the cathode channel to the anode channel. Hydrogen at anode channel reacts on the carbonate ion moving from the cathode channel. Also, WGSR rebalances the anode gas mixture composition at the same time. Figure 2.2 shows species flows in the fuel cell. The following reactions are the electrochemical reactions in the fuel cell.

Reforming channel: $CH_4 + 2H_2O \rightarrow aH_2 + bCO_2 + cCO + dH_2O$

Water-gas shift reaction: $CO + H_2O \leftrightarrow H_2 + CO_2$

Anode: $H_2 + CO_3^{2-} \rightarrow H_2O + CO_2 + 2e^-$

Cathode: $(1/2)O_2 + CO_2 + 2e^- \rightarrow CO_3^{2-}$

The fuel cell model is divided into 25 segments in the direction of anode

and cathode flows. Figure 2.3 (a) shows 25 segments and (b) shows energy and mass flow at each segment. As shown Figure 2.3, there are isothermal part and non-isothermal part in each segment. At isothermal part, which is state 1 and state 2, electrochemical reactions occur. The current density is determined based on the operating cell voltage and the calculated irreversible losses. WGSR equilibrates the composition of anode gas mixture. At non-isothermal part, which is state 3, the segment temperature is calculated by considering exothermicity Qisothermal,i from isothermal part and heat transfer Qref,i by reforming process, which is endothermic.

Figure 2.4 shows the algorithm flow chart of MCFC modeling. Firstly, fuel cell operating voltage is assumed. As mentioned above, each segment is divided into isothermal part and non-isothermal part. At isothermal part, current density and work output of each segment is calculated on the basis of the operating voltage. At non-isothermal part, heat balance is computed and then temperature of next segment is determined. After processing at 25 segments, total current and work output is determined and utilization factor is calculated on basis of lower heating value of fuel and anode off-gas. If the utilization factor doesn't match with desired value, the procedure is iterated on basis of new assumed operating voltage. Detailed modeling process for the fuel cell is obtained in Ref. [13] or Appendix A.

2.3. HCCI engine modeling

HCCI engine model was developed by authors in Refs. [13, 17, 18]. This model is coded by MATLAB and Cantera toolbox, which allows the chemical reaction kinetics calculation. GRI 3.0 chemical reaction mechanism is adopted. The mechanism contains 53 species and 325 reactions. And the mechanism is optimized for natural gas reaction [19]. During compression, power and expansion strokes, heat transfer is calculated by using woschni model.

The model assumes the followings.

- In-cylinder mixture is a homogeneous thermodynamic state.
- Compression, power and expansion strokes are considered except intake and exhaust processes.

The HCCI model doesn't consider intake and exhaust processes, and thus excludes the pumping losses from gas exchange processes. Nevertheless, the results have been reflecting on general trend like typical HCCI engine. However, applying the turbocharger, engine intake and exhaust charge pressures are not same. In this case, the engine net power output is calculated by considering the pumping loss, which is calculated by using the difference between the pressures of the engine intake and exhaust charge.

Table 2.1 shows the engine model geometry and operating conditions. The

engine geometry is determined by reference to commercialized Cummins KTA 50 engine. Equivalence ratio '1' means stoichiometric state, which means engine is supplied enough oxygen to completely combust carbon monoxide and hydrogen of anode off-gas.

The HCCI engine model has some strategies for complete combustion. The followings are the strategies. The combustion efficiency should be not less than 98%. The combustion efficiency is defined as Eqn. 2.1

$$\eta_c = 1 - \frac{LHV_{out}}{LHV_{in}} \qquad (2.1)$$

LHV_{in} is the lower heating value of fuel supplied, and LHV_{out} is the lower heating value of the exhaust gas. The efficiency is controlled by engine intake charge temperature. The temperature increases for high combustion efficiency. However, if temperature increases largely, the combustion timing is too early, and thus the engine performance may be worse. For the proper combustion timing, maximum pressure rise rate was kept between about -10 CAD bTDC and 10 CAD aTDC. Using these strategies, the combustion can occur at an appropriate timing.

2.4. Turbocharger modeling

Turbocharger is originally used for increasing engine power output. The turbocharger consists of compressor and turbine. Compressor is located in front of HCCI engine and turbine is placed behind the engine. Compressor

compresses engine inlet gas and then the amount of high pressure gas entering the engine is more. For the reason, engine yields more power output. Engine exhaust gas enters the turbine. The turbine yields power output and then the power output is transmitted to the compressor. In this study, turbocharger is used to downsize the engine. More amount of gas doesn't enter the engine, but same amount of the gas enters the downsized engine. The system size is miniaturized and costs of the system would be reduced.

In this study, turbocharger modeling is used to examine the possibility of downsizing the engine. Accordingly, it was analyzed using a simple turbocharger model. This model is in reference to Ref. [20] by Moraal et al., and the main governing equations are reproduced as followings with some modifications.

PR is the pressure ratio of the compressor. If PR is defined, the pressure of the gas discharged the compressor is calculated as Eqn. 2.2.

$$P_{c,out} = PR \times P_{c,in} \qquad (2.2)$$

where $P_{c,out}$ is the discharged gas pressure from the compressor, and $P_{c,in}$ is the pressure of the compressor inlet gas.

The compressor needs power to be operated. The power is given by Eqn. 2.3.

$$W_c = \dot{m}_c c_p (T_{c,out} - T_{c,in}) \qquad (2.3)$$

where $\dot{m}_c$ is the mass flow rate of the gas entering the compressor, c_p is

the specific heat of the gas, and $T_{c,in}$, $T_{c,out}$ are the temperature of compressor inlet and outlet.

For assuming isentropic process, the relation between the temperature and the pressure is as followings.

$$\frac{T_{c,out,s}}{T_{c,in}} = \left(\frac{P_{c,out}}{P_{c,in}}\right)^{\frac{r-1}{r}} \qquad (2.4)$$

where $T_{c,out,s}$ is the temperature of the gas discharged the compressor at isentropic process, $T_{c,in}$ is the temperature of the compressor inlet gas, and r is the ratio of specific heat of the gas.

For substantial results, isentropic efficiency is introduced as Eqn. 2.5, and real temperature of the compressor outlet is calculated as Eqn. 2.6.

$$\eta_{c,s} = \frac{T_{c,out,s} - T_{c,in}}{T_{c,out} - T_{c,in}} \qquad (2.5)$$

$$\frac{T_{c,out}}{T_{c,in}} = 1 + \frac{\left(\left(\frac{P_{c,out}}{P_{c,in}}\right)^{\frac{r-1}{r}} - 1\right)}{\eta_{c,s}} \qquad (2.6)$$

where $\eta_{c,s}$ is isentropic efficiency, and $T_{c,out}$ is real temperature of the compressor outlet. In this study, the isentropic efficiency of the compressor is assumed to be 70%.

It is possible to determine the actual work using the efficiency. The work is more than that of isentropic process, and is given by Eqn. 2.7.

$$W_c = \frac{\dot{m}_c c_p T_{c,in}\left(\left(\frac{P_{c,out}}{P_{c,in}}\right)^{\frac{r-1}{r}} - 1\right)}{\eta_{c,s}} \quad (2.7)$$

The exhaust gas of the engine enters the turbine, and the gas of the normal pressure is discharged from the turbine. During this period, the turbine yields power output. The power output is given by Eqn. 2.8.

$$W_t = \dot{m}_c c_p (T_{t,in} - T_{t,out}) \quad (2.8)$$

where $\dot{m}_t$ is the mass flow rate of the gas passing through the turbine, and $T_{t,in}$, $T_{t,out}$ are the temperature of the turbine inlet and outlet.

At isentropic process, the pressure and the temperature of the turbine gas are as following Eqn. 2.9.

$$\left(\frac{P_{t,in}}{P_{t,out}}\right)^{\frac{r-1}{r}} = \frac{T_{t,in}}{T_{t,out}} \quad (2.9)$$

where $P_{t,in}$ and $P_{t,out}$ are the pressure of the turbine inlet and outlet, and $T_{t,out,s}$ is the temperature of turbine outlet at isentropic process.

The isentropic efficiency of the turbine is given by Eqn. 2.10. Using the efficiency, the temperature of the turbine outlet is calculated as shown in Eqn. 2.11.

$$\eta_{t,s} = \frac{T_{t,in} - T_{t,out}}{T_{t,in} - T_{t,out,s}} \quad (2.10)$$

$$T_{t,out} = T_{t,in}\left(1 - \eta_{t,s}\left(1 - \left(\frac{P_{t,out}}{P_{t,in}}\right)^{\frac{r-1}{r}}\right)\right) \quad (2.11)$$

where $T_{t,out}$ is the temperature of the turbine outlet at real process, and

the isentropic efficiency of the turbine is assumed to be 70%.

The power output of the turbine is given by Eqn. 2.12 using Eqn. 2.8-2.11.

$$W_t = \dot{m}_t c_p \eta_{t,s} T_{t,\in} \left(1 - \left(\frac{P_{t,out}}{p_{t,in}} \right)^{\frac{r-1}{r}} \right) \qquad (2.12)$$

Finally, the power yielded by the turbine is partially transmitted to the compressor for mechanical loss. The mechanical efficiency is given by Eqn. 2.13 and the value is assumed to be 80%.

$$\eta_m = \frac{W_c}{W_t} \qquad (2.13)$$

Table 2.1 Engine geometry and operating conditions

Bore (mm)	145
Stroke (mm)	145
Cylinders	8
Displacement (L)	19.2
Compression ratio	12.5
Engine speed (rpm)	1800
Equivalence ratio	1 (Stoichiometric)

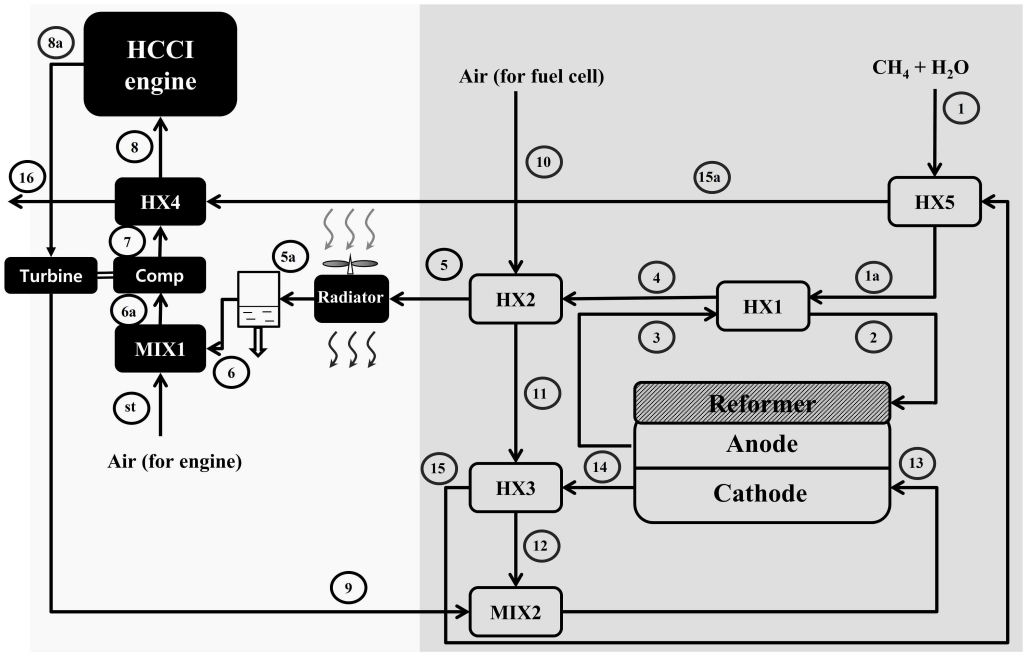

Figure 2.1 New hybrid system configuration

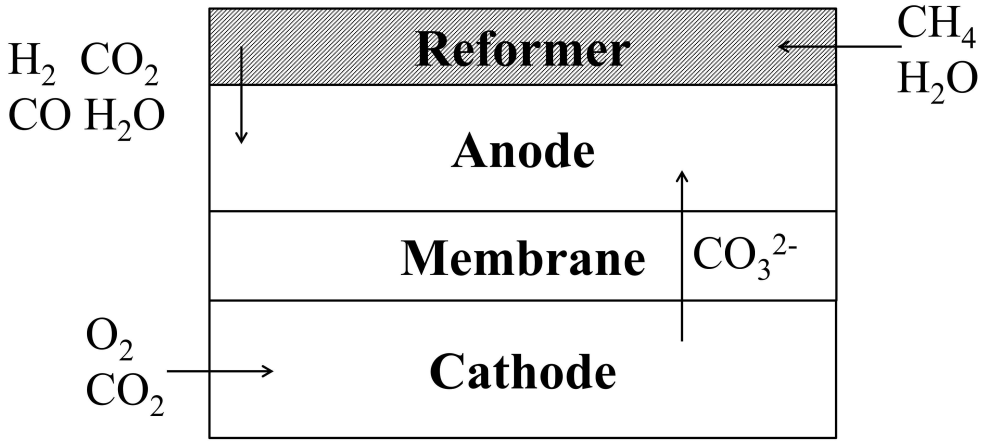

Figure 2.2 Species flows in MCFC stack

(N2 and H2O omitted at cathode)

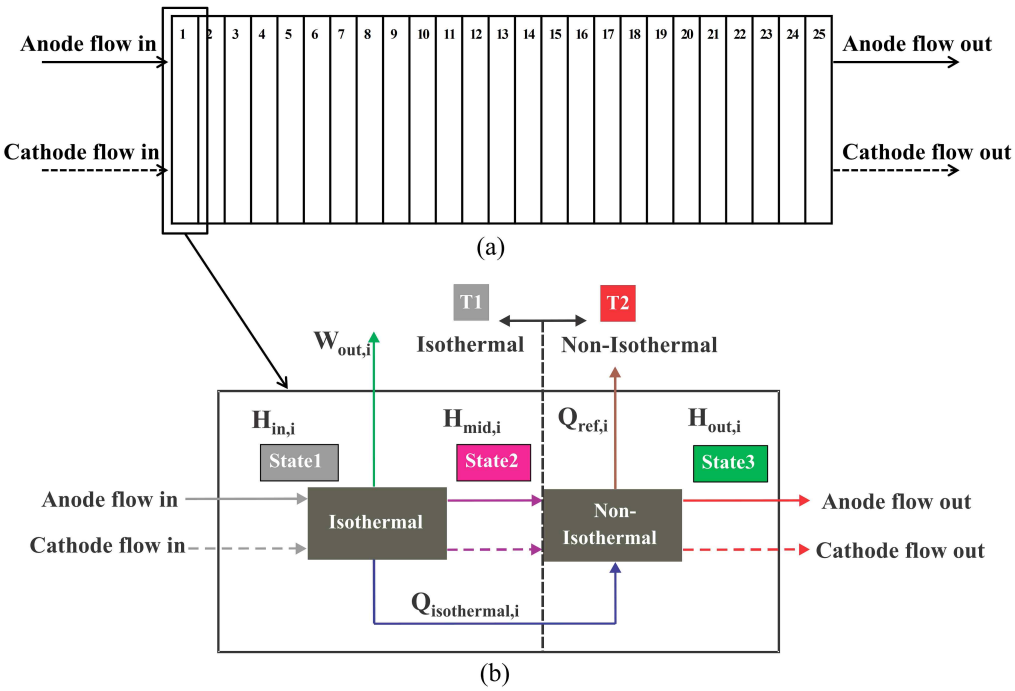

Figure 2.3 MCFC stack modeling schematic (a) Parallel flows with 25 segments and (b) Energy flows within each segment

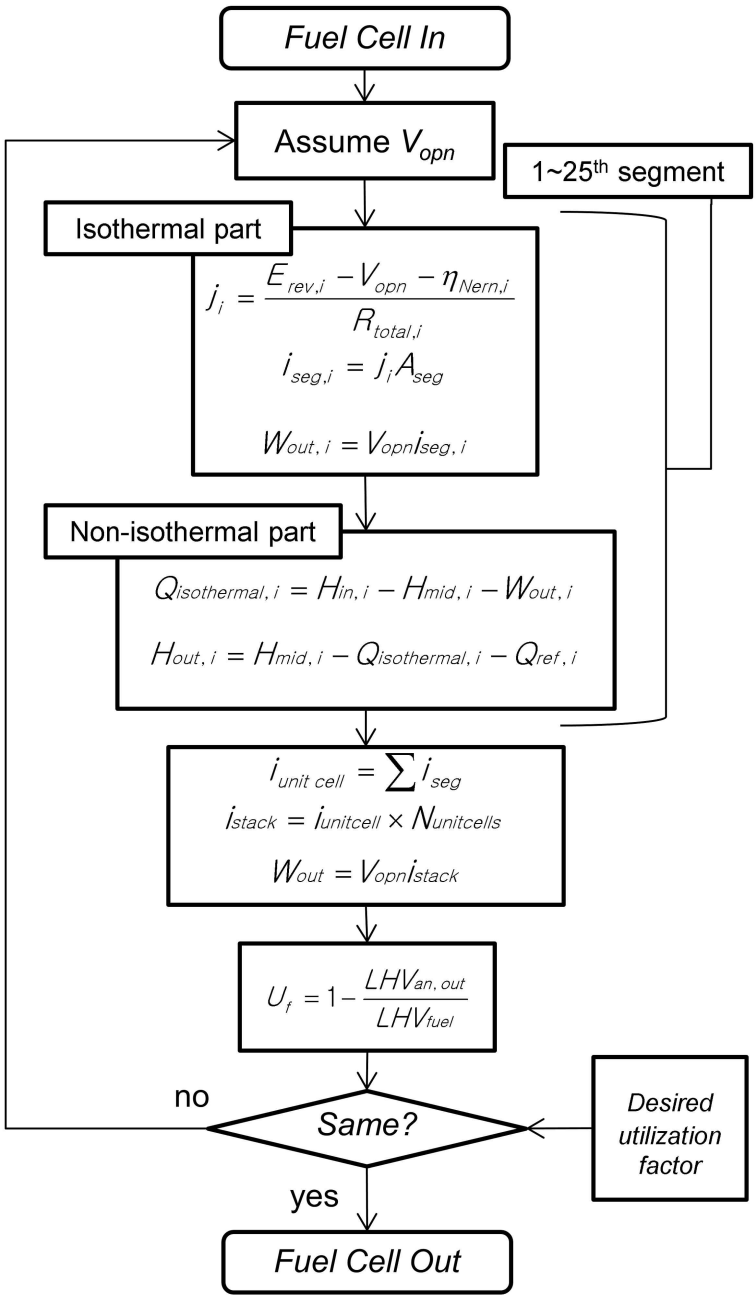

Figure 2.4 MCFC stack modeling flow chart

3. Engine Downsizing

As discussed in Section 1, engine downsizing is needed to reduce the cost as well as to increase the specific power output of the engine in the hybrid system. In our previous work, the HCCI engine has a displacement volume of 18.4 liter, while producing only 55 kW at design point operation [13]. This is only ~$1/10^{th}$ of the typical power that the engine of similar size can deliver. In this section, two strategies are suggested to downsize the engine by reducing the volume flow rate in a given mass flow rate from the fuel cell to the engine. In Section 3.1, the use of turbocharger for the engine operation is demonstrated to increase the intake charge pressure of the engine, and in Section 3.2, the higher geometric compression ratio of the engine is exploited to decrease the required intake charge temperature and thus reduce the volume flow rate.

3.1. Increasing pressure of engine intake charge – Turbocharger

In this section, increasing pressure of engine intake charge is discussed as one of the methods to downsize the engine in the hybrid system. Figure 3.1 is the same as Figure 2.1 in Section 2, and is reproduced here for showing the streams. The volume of the intake charge (state 8) is decreased with the same mass flow rate, as the pressure of the gas is

increased. To raise the pressure of the gas, either turbocharger or supercharger is a promising candidate. The turbocharger consists of compressor and turbine interconnected by a shaft. In the turbine, engine exhaust charge at high temperature and pressure expands into atmospheric pressure and relatively lower temperature state. The work is generated during this expanding process and is transmitted to the compressor through the shaft. The compressor raises the pressure of the engine intake charge, typically from the ambient pressure, and then the high pressure gas enters the engine. Due to the temperature rise during the compression process, it is common to have the intercooler installed between the compressor outlet and the engine intake, in order to cool the charge down. The higher pressure of the intake charge leads to the lower volume flow rate of the intake charge in a given mass flow rate, and thus the required volume of the engine in the hybrid system can be reduced. On the other hand, the supercharger is simply a compressor, which is powered by using some portion of the engine work output. The supercharger may also have an associated intercooling system. Compressing the intake charge by the supercharger has the same effect as by the turbocharger. However, while the compressor of the turbocharger doesn't require additional power than the one transferred from the companion turbine, supercharger demands extra work from the engine itself and thus there is an efficiency penalty. In this study, we are

focusing on the turbocharger application, because the main goal of the hybrid system is to maximize the system efficiency. In the following sections, under various boosting pressures by turbocharger, the component performances, i.e. MCFC and HCCI engine are described, followed by the discussion on the system performances.

3.1.1. Component characteristics under pressure ratio variation - MCFC stack

As explained above, the compressor is placed in front of the engine, and pressurizes the intake charge. The "pressure ratio (PR)" is defined as the ratio of the compressor exit and inlet pressures of the gas. In this study, the hybrid system including the HCCI engine with turbocharger is analyzed under various PR's, from 1.25 to 2.5. To isolate the effect of MCFC on the system performances under this variation, MCFC anode inlet (state 2) and cathode inlet (state 13) condition have been kept the same, of which the temperatures are controlled by the amount of heat exchange in HX1 and HX3, while keeping the maximum effectiveness of the heat exchangers under 85%. The fuel (CH4) supply rate and steam-to-carbon ratio are fixed at 500 kW (LHV basis) and 2.5:1, respectively. As a result, MCFC power output is almost the same of 260 kW though the pressure ratio is changed, as shown in Figure 3.2.

3.1.2. Component characteristics under pressure ratio variation – HCCI engine

As discussed in Section 2.3, in HCCI engine, certain intake charge temperature is required to achieve the proper combustion timing and the complete combustion. In this study, the combustion timing is represented by maximum pressure rise rate, which was kept between about -10 CAD bTDC and 10 CAD aTDC. For complete combustion, combustion efficiency over 98% was ensured. The combustion efficiency (η_c) is defined as the ratio of the lower heating value of fuel consumed in the engine to the lower heating value of fuel supplied.

Figure 3.3 shows the engine intake charge temperature for various pressure ratios. At pressure ratio of 2.5, the requirement of the engine intake charge temperature need to increase. As mentioned in Section 2.3, the requirement of the engine intake charge temperature is decided by satisfying the combustion efficiency of 98%. However, at pressure ratio of 2.5, the engine exhaust charge temperature is not enough high to satisfy the MCFC cathode inlet temperature if the engine intake charge temperature is decided for the requirement. Accordingly, the engine intake charge temperature increases more than the requirement. The engine exhaust charge temperature also rises, and thus satisfies the MCFC cathode inlet temperature. Except the pressure ratio of 2.5, the engine intake charge temperature decreases a little, as the pressure ratio is

increased. This is mainly because overall higher pressure of the mixture leads to shorter ignition delay, which should be compensated by slightly lowered temperature to keep the similar HCCI combustion timings. Figure 3.4 shows the combustion timings. The combustion timing of '0' means that the gas mixture in cylinder combusts at TDC. The combustion timing of '-10' means a combustion at 10 bTDC, and the '10' means a combustion at 10 aTDC. The results are similar as the pressure ratio changes except the PR 2.5. The combustion timing at PR 2.5 is faster than that at other PR because the engine intake charge temperature is higher than the requirement for satisfying the combustion efficiency of 98%. And Figure 3.5 shows that the combustion efficiency is always more than 98%. It is noted that the engine intake temperature is controlled by changing the amount of heat exchange in HX4. Although there is slightly increase in temperature through the compressor, it is still not reaching the required temperature and the additional heating is needed in HX4.

Figure 3.6 depicts the turbine exhaust temperature, which shows also same trend to the intake temperature in Fig. 3.3. The turbine exhaust charge is same with total engine system exhaust charge. The turbine exhaust charge temperature (state 9) is also lower as the pressure ratio increases. The gas in engine is compressed and expanded, so temperature of the total engine system exhaust gas is also low if temperature of the engine inlet gas is low.

Since the fuel cell system is known for its cleanness in pollutant emissions, it is desirable that the addition of an HCCI engine to the fuel cell system should not cause any additional harmful emissions. Major pollutants considered in typical internal combustion engine are unburned hydrocarbons (UHC), carbon monoxide (CO), and oxides of nitrogen (NOx). Among these, the first two components are difficult to be estimated in our zero-dimensional engine modeling, because in-cylinder geometry, especially the crevice volume around the piston, should be considered to accurately estimate it. However, for the production of oxides of nitrogen, the peak temperature during combustion process is known to be the most determining factor, and the production rate exponentially increases above ~1800 K. Figure 3.7 shows the peak temperatures for the tested conditions, and they are all around 1700 K, very much under 1800 K. This low peak temperature is due to the diluted nature of the anode-off gas where only small amount of fuel chemical energy is left for the combustion in the HCCI engine. Therefore, it is expected that there is almost no NOx in the exhaust gas of the HCCI engine for the hybrid system operation.

Figure 3.8 shows peak pressure during the combustion process. The peak pressure increases almost linearly as the pressure ratio of the compressor rises. Because the engine geometric compression ratio is fixed at 12.5 and the anode-off gas contains similar amount of fuel chemical energy left for

the HCCI combustion, the peak pressure in the engine is increased as the intake charge pressure is increased by the compressor. At pressure ratio of 2.5, the peak pressure in the engine is already over 80 bar, which may be detrimental to the mechanical parts during the real engine operation, and thus no more compression above this point is tested in our simulation study, either.

Figure 3.9 shows almost constant engine power output as the pressure ratio varies. Although a turbocharger in an IC engine is typically intended to increase the power output in a given engine size, it is reminded that our purpose of using the turbocharger is to downsize the engine for a given mass flow rate from the fuel cell by increasing the intake charge pressure.

Figure 3.10 shows the downsizing ratio of the engine displacement volume, where the 100% point corresponds to 19.2 L of the HCCI engine in the original hybrid system without turbocharger. Downsizing by a turbocharger proves itself to be an effective way, in that the pressure ratio of 1.25 already achieves 75% engine downsizing. The engine size falls below 40% at the highest pressure ratio tested, which implies that the final engine size is ~7.68 L, as compared to 19.2 L without turbocharger.

3.1.3. System performance

Figure 3.11 and 3.12 show the net power output and efficiency of the hybrid system as a whole. As already described in Sections 3.1.1 and 3.1.2, the power outputs of the fuel cell and the engine are almost constant, and thus those of hybrid system are not changing much as the compressor pressure ratio (PR) changes.

In summary, a turbocharger was successfully applied to the hybrid system without changing overall system performances, while maximizing the potential of engine downsizing. Still, the peak pressure during the engine operation should be considered when determining the maximum pressure ratio, and the off-design operation with this additional degree of freedom should be carefully examined. This last point will be discussed in details in Section 4.

3.2. Decreasing temperature of engine intake charge

In this section, new engine design is suggested to reduce the intake charge temperature requirement for downsizing. As the temperature of the gas is decreased, the volume flow rate for a given mass flow rate is decreased due to an increase in the density of the gas. However, when the intake charge temperature is lowered, the ignition delay of the mixture becomes longer and, at certain minimum intake temperature condition, the engine will suffer incomplete combustion or even misfire.

To remedy it, the increase in geometric compression ratio of the HCCI engine is suggested. At higher compression ratio, the mixture can achieve the comparable post-compression temperature and pressure with lower intake temperature than otherwise. It is noted that the geometric compression ratio is not a variable that can be changed during the operation, but should be designed and implemented when the engine is manufactured. In the following sub-sections, the components and system performances under various geometric compression ratio of the HCCI engine are discussed.

3.2.1. Component characteristics under compression ratio variation - MCFC

The geometric compression ratio (CR) of the engine in our previous hybrid system was 12.5, which was chosen to match the typical compression ratio of the gasoline-fueled HCCI engine. In this study, for downsizing purpose, the geometric compression ratio is increased up to 22.5, which is somewhat higher value than that of the conventional diesel-fueled compression ignition engine.

The operating conditions for the geometric compression ratio variation are shown in Table 3.2. To isolate the effect of the fuel cell under CR variation, the amount of fuel entering the fuel cell, fuel utilization factor, and steam-to-carbon ratio are the same for all the tested conditions. In

addition, anode inlet (state 2) and cathode inlet (state 13) conditions are kept almost constant. As a result, MCFC power output is almost the same at 260 kW, as shown in Fig. 3.13. To control the inlet temperatures for the fuel cell, the amounts of heat exchange in HX1 and HX3 are adjusted. Effectiveness of all the heat exchangers is still kept under 85%.

3.2.2. Component characteristics under compression ratio variation - HCCI engine

Figure 3.14 shows the engine intake charge temperature for various geometric compression ratios. As mentioned in the preceding section, intake temperature can be lowered almost linearly with the compression ratio. These temperatures were selected as the minimum temperature to ensure the combustion efficiency over 98%, and controlled by changing the amount of heat exchange in HX4. Only for the highest CR tested, the temperature couldn't be lowered much further, and the reason will be discussed below.

The engine exhaust gas temperature shows similar trends as the intake temperature, as shown in Fig. 3.15. As shown in Fig. 3.1, the engine exhaust charge temperature (state 9) is important to achieve the required MCFC cathode inlet temperature (state 13). If the engine exhaust gas temperature is low, there should be more heat exchange in HX3, and thus require higher effectiveness to preheat the cathode air before mixing. We

found out that at CR of 22.5, to keep the effectiveness of HX3 under 85%, the engine inlet temperature couldn't be decreased much further, as shown in Fig. 3.14, to keep the exhaust temperature at the present level in Fig. 3.15. In this way, the HX3 effectiveness was kept under 85% and the cathode inlet temperature was around 580°C.

Figure 3.16 shows peak temperature during combustion. The temperatures are similar at various compression ratios, because the lowered intake temperature with higher CR is compensated by more compression during the main compression stroke. The peak temperatures are all less than 1800 K, thus the very low NOx emissions are expected.

When the geometric compression ratio is higher, it is evident that the peak pressure during the combustion is higher, as shown in Fig. 3.17. At CR of 22.5, the peak pressure increases faster, and it is due to faster combustion timing as shown in Fig. 3.18. At CR of 22.5, the engine intake charge temperature is not reduced to a minimum temperature for ensuring the combustion efficiency over 98% as mentioned above. Thus, the combustion timing is also faster, and the peak pressure in the engine is higher.

In a typical engine, the higher the compression ratio is, the higher the engine efficiency is. Since the anode-off gas is almost the same for all the tested conditions, this higher efficiency leads to higher power output, as shown in Fig. 3.19. However, the engine power output and efficiency

may be reduced if the compression ratio is too high. The reason is that heat transfer increases rapidly due to a high surface-to-volume ratio near TDC.

3.2.3. System performance

Figure 3.20 shows the potential of the downsizing by the increased geometric compression ratio. We set the displacement volume of the engine at CR of 12.5 as the downsizing ratio of 100%. At CR of 22.5, the engine displacement volume is about 16.5 L which is ~14% reduction, as compared to the one at CR of 12.5.

Since the fuel input and MCFC operating conditions are fixed as mentioned earlier, net MCFC output is almost the same. Engine output and engine efficiency are gradually increased with higher compression ratio for the reason mentioned in Section 3.2.2. Accordingly, hybrid system power output and efficiency are also increased, as shown in Figs. 3.21 and 3.22.

Finally, it is interesting to note the variation of the hybrid system outlet (state 16) temperature, as shown in Fig. 3.23. It is the final exhaust temperature from the system, which can be exploited in combined heat application. The temperature is decreased with higher CR, which is mainly because the engine power output, and thus the system output, increases for a given fuel chemical energy supplied to the system. However, the

temperature at CR 22.5 is still high at ~560 K enough to be used as heat source for bottoming applications.

In summary, the proper selection of the engine geometric compression ratio can be a way to downsize the engine. However, the downsizing ratio under reasonable CR variation is somewhat limited, as compared to the use of turbocharger in Section 3.1. There is a small benefit with high CR operation that the HCCI engine efficiency and power output increases a bit, but the penalty on the peak pressure should be considered, when the compression ratio is decided.

Table 3.1 MCFC operating conditions under pressure ratio variation

Parameter	PR 1.0	PR 1.25	PR 1.5	PR 1.75	PR 2.0	PR 2.25	PR 2.5
LHV CH_4(kW)	500						
Fuel utilization factor (%)	70						
Air utilization factor (%)	40						
S/C ratio (H_2O:CH_4)	2.5 : 1						
Anode inlet temperature (°C)	571	569	571	571	571	571	569
Cathode inlet temperature (°C)	581	582	578	578	578	578	579

Table 3.2 MCFC operating conditions under compression ratio variation

Parameter	CR 12.5	CR 15	CR 17.5	CR 20	CR 22.5
LHV CH_4(kW)	500				
Fuel utilization factor (%)	70				
Air utilization factor (%)	40				
S/C ratio (H_2O:CH_4)	2.5 : 1				
Anode inlet temperature (°C)	571	571	571	571	571
Cathode inlet temperature (°C)	581	579	579	578	579

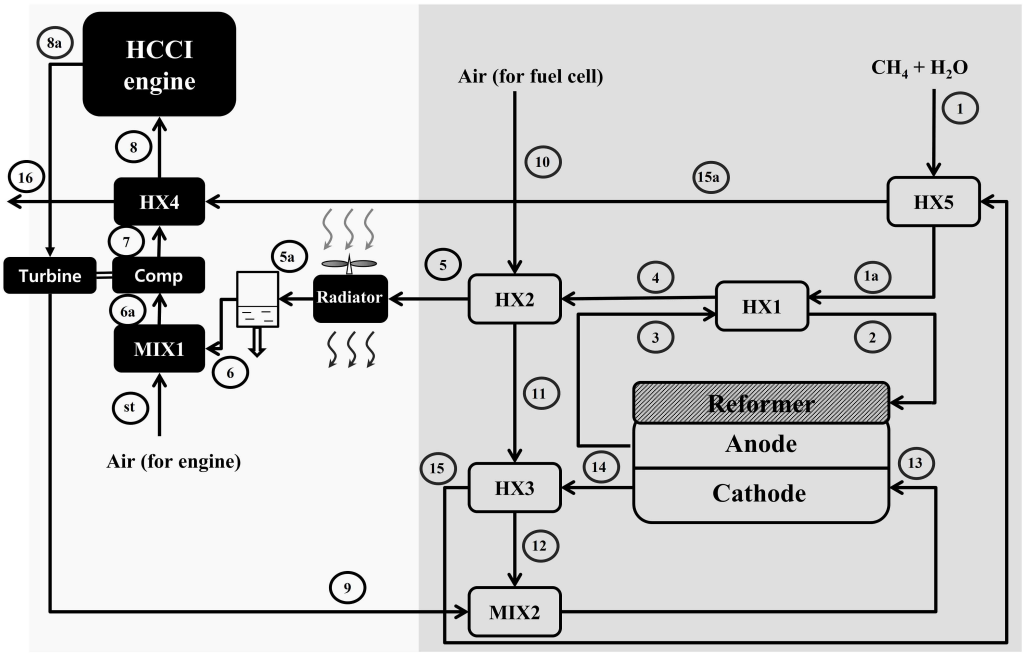

Figure 3.1 New hybrid system configuration (reproduced)

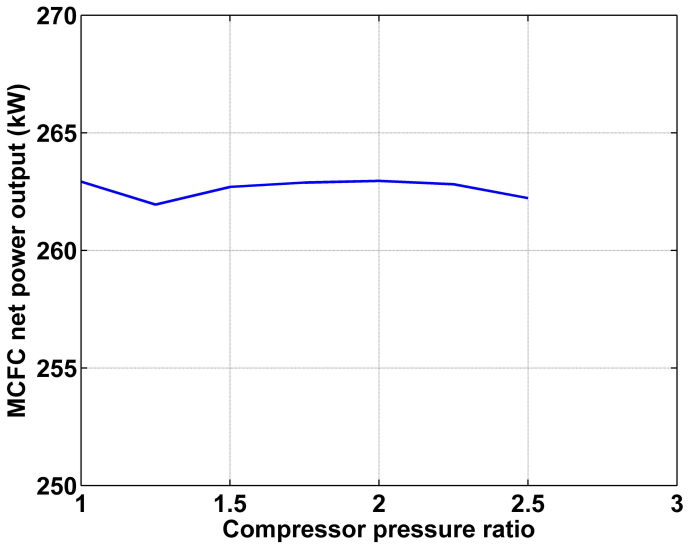

Figure 3.2 MCFC net power output under pressure ratio variation

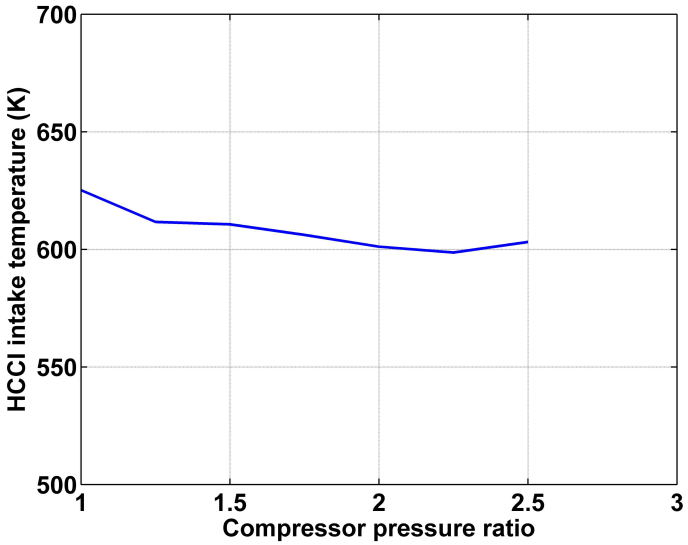

Figure 3.3 HCCI engine intake charge temperature under pressure ratio variation

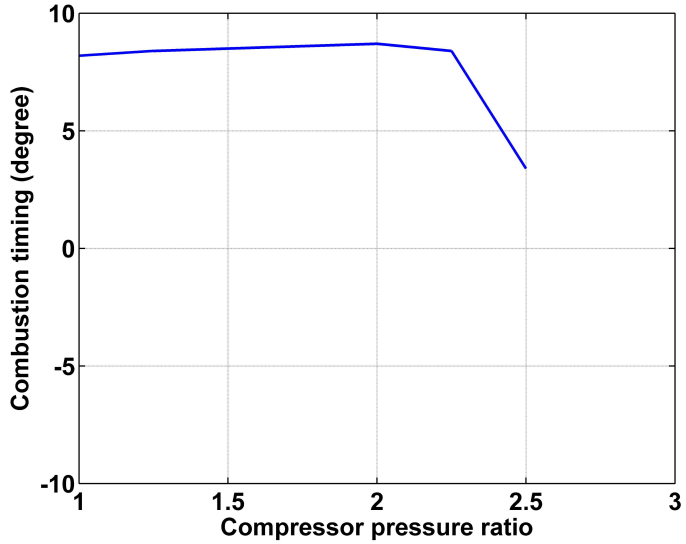

Figure 3.4 Combustion timing in HCCI engine under pressure ratio variation

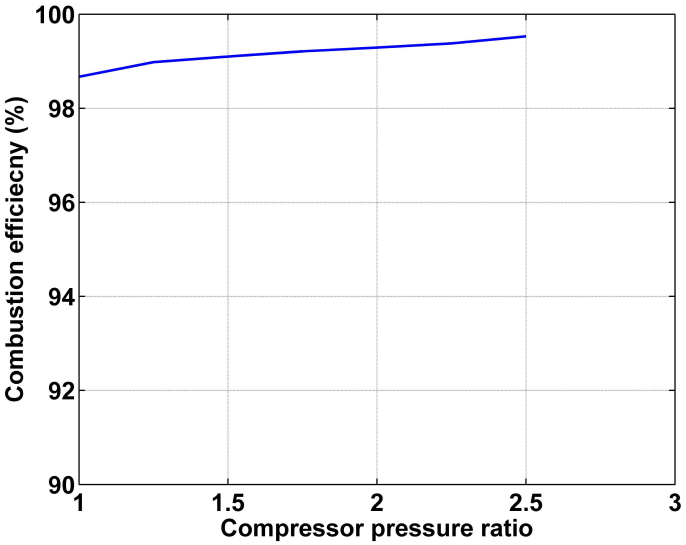

Figure 3.5 Combustion efficiency in HCCI engine under pressure ratio variation

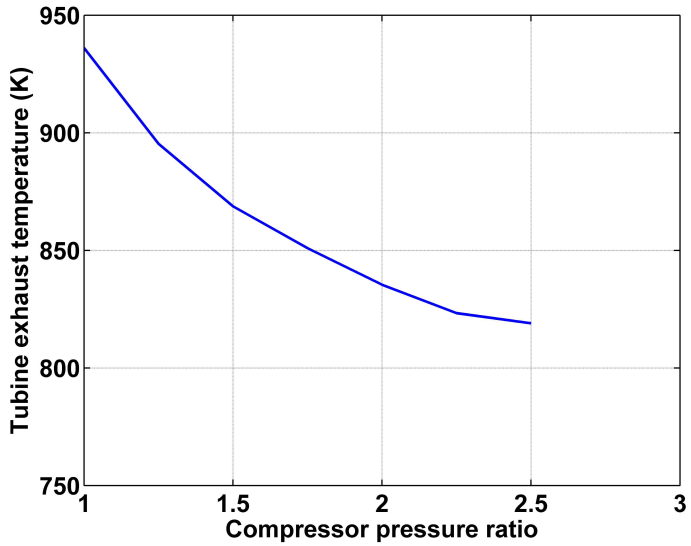

Figure 3.6 Turbine exhaust charge temperature under pressure ratio variation

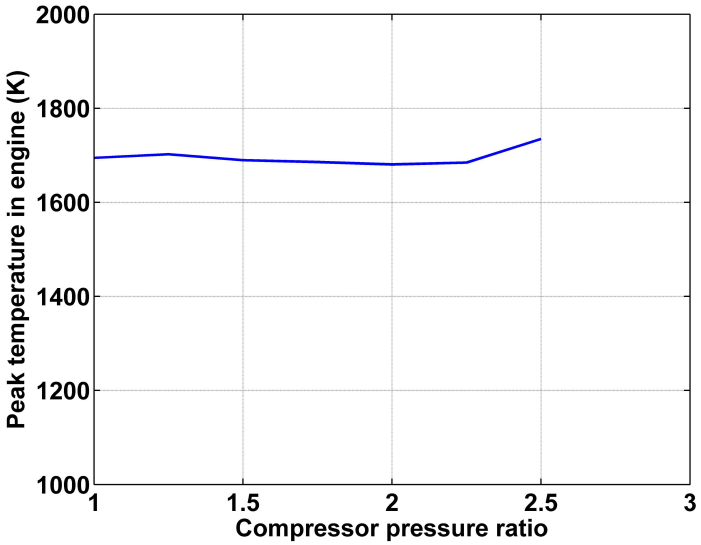

Figure 3.7 Peak temperature in HCCI engine under pressure ratio variation

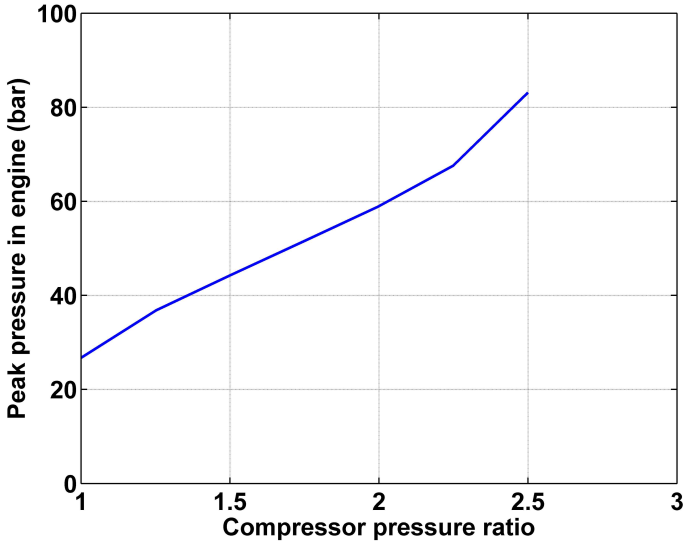

Figure 3.8 Peak pressure in HCCI engine under pressure ratio variation

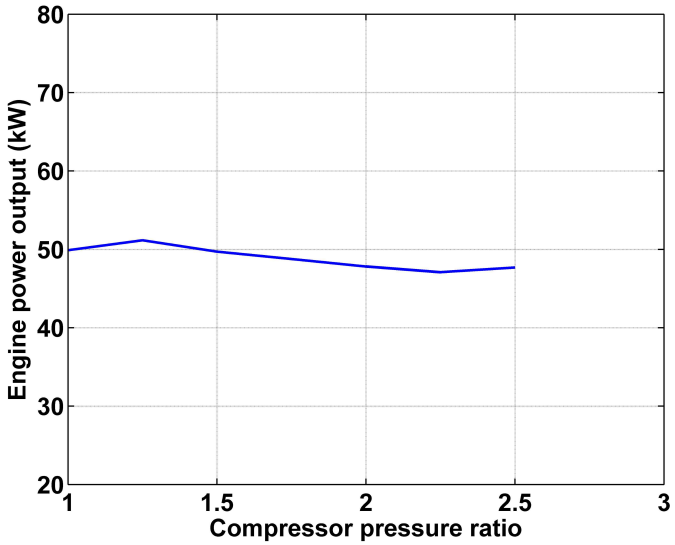

Figure 3.9 HCCI engine power output under pressure ratio variation

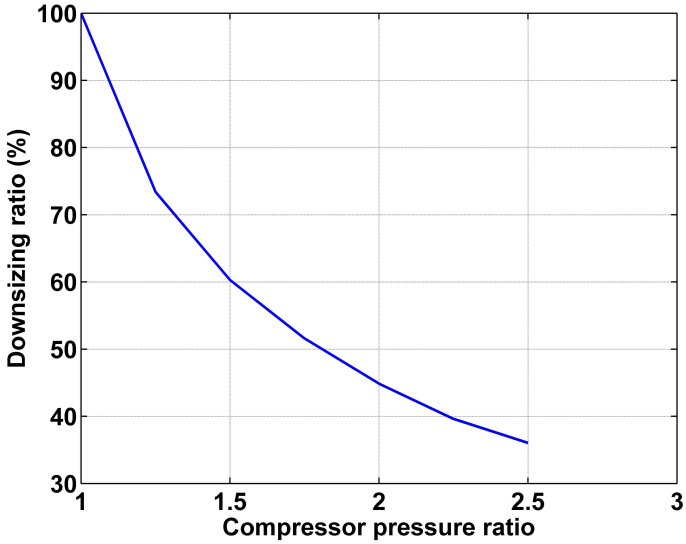

Figure 3.10 HCCI engine downsizing ratio under pressure ratio variation

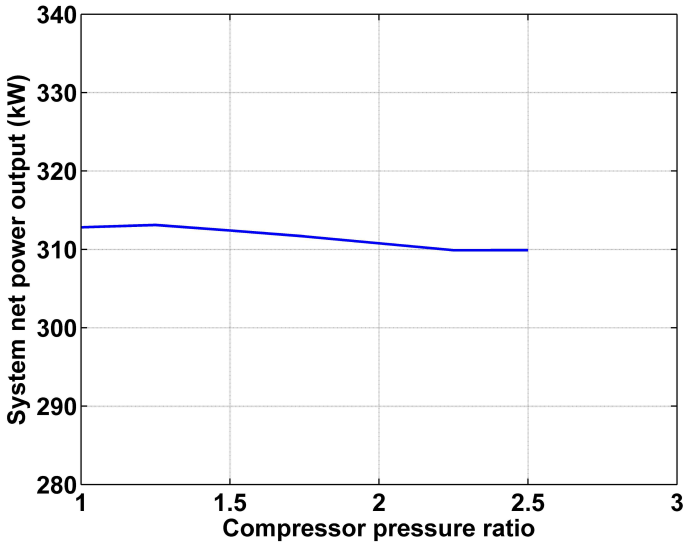

Figure 3.11 Overall system net power output under pressure ratio variation

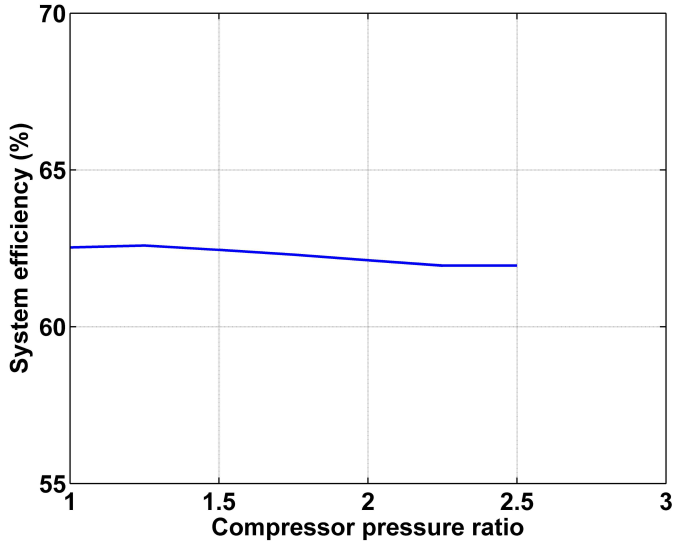

Figure 3.12 Overall system efficiency under pressure ratio variation

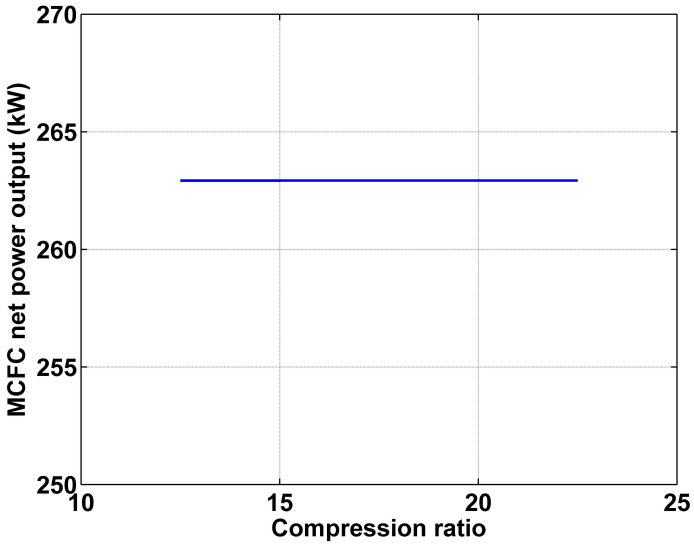

Figure 3.13 MCFC net power output under compression ratio variation

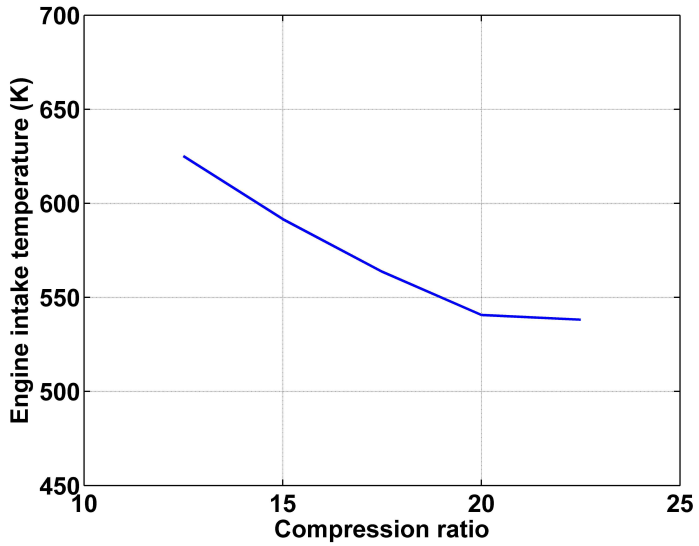

Figure 3.14 HCCI engine intake charge temperature under compression ratio variation

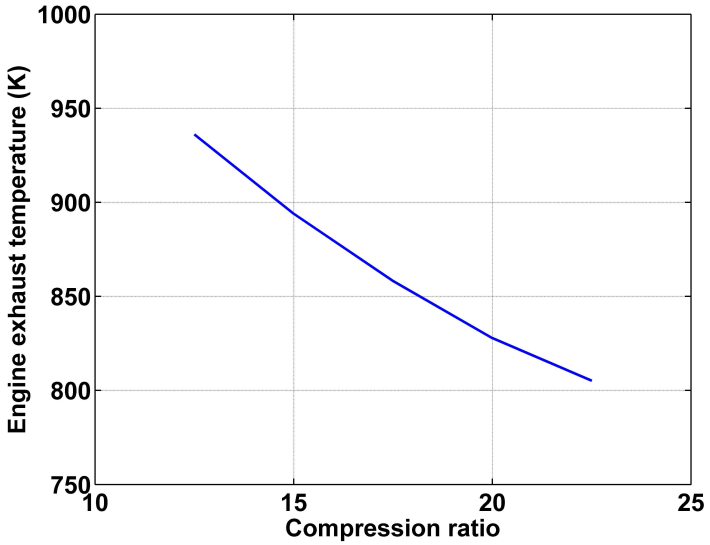

Figure 3.15 HCCI engine exhaust charge temperature under compression ratio variation

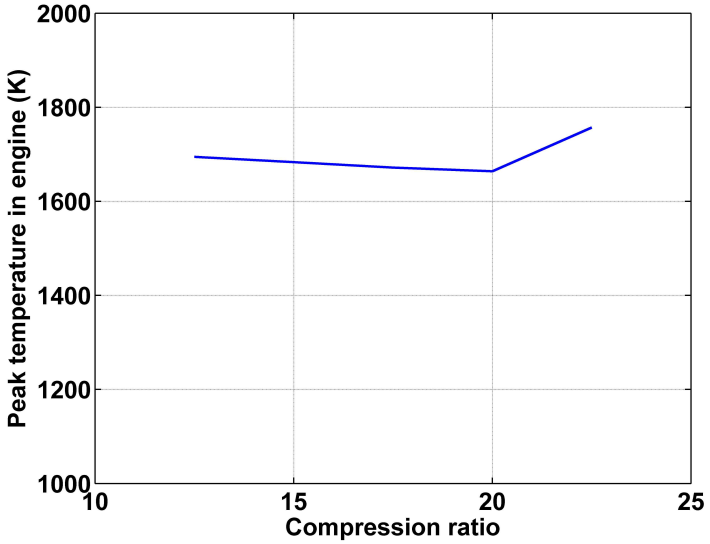

Figure 3.16 Peak temperature in HCCI engine under compression ratio variation

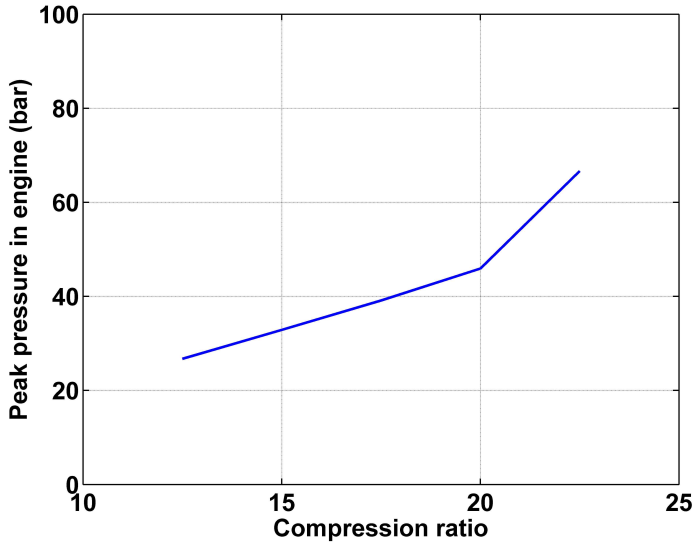

Figure 3.17 Peak pressure in HCCI engine under compression ratio variation

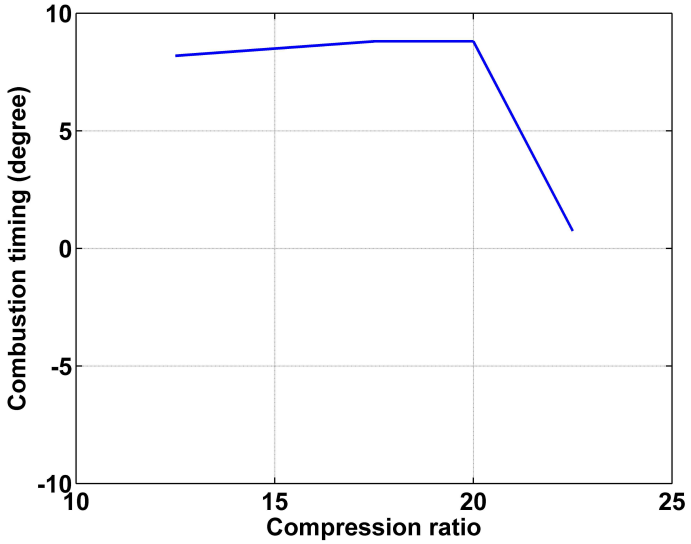

Figure 3.18 Combustion timing in HCCI engine under compression ratio variation

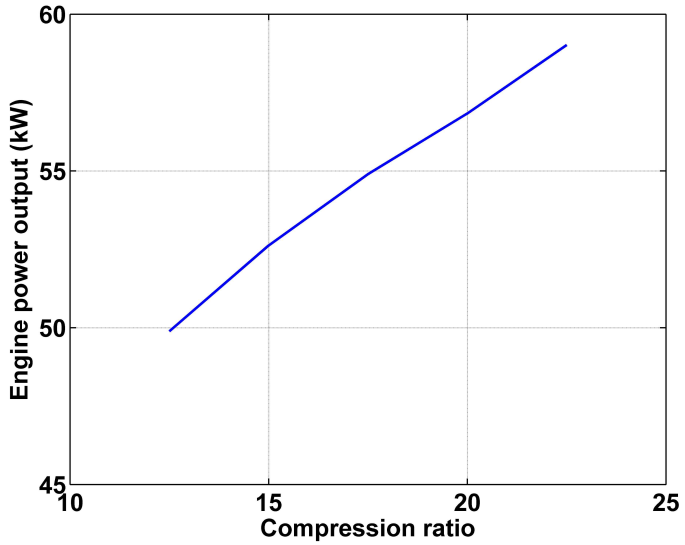

Figure 3.19 HCCI engine power output under compression ratio variation

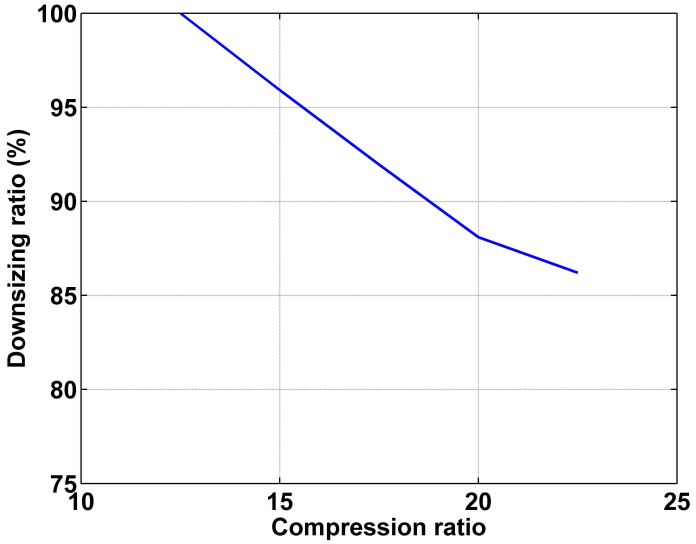

Figure 3.20 HCCI engine downsizing ratio under compression ratio variation

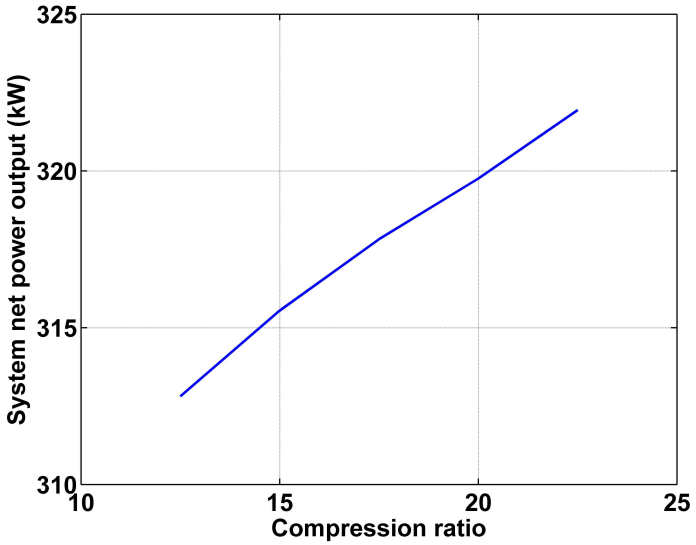

Figure 3.21 Overall system power output under compression ratio variation

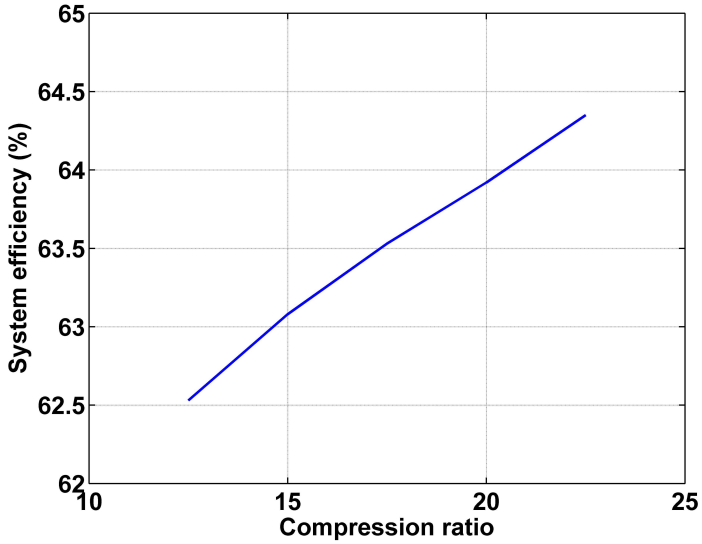

Figure 3.22 Overall system efficiency under compression ratio variation

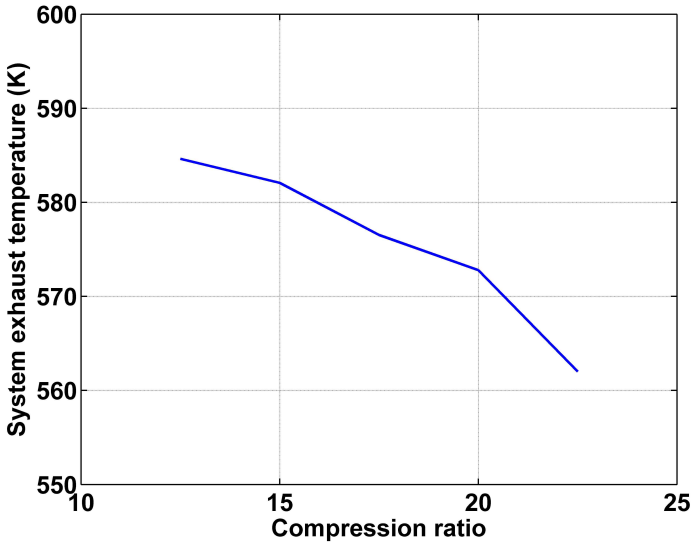

Figure 3.23 Overall system exhaust temperature under compression ratio variation

4. Off-design Operation

In this section the strategy to operate the hybrid system at off-design conditions is discussed. In general, the power-generating system runs at constant power output for most of its life-time, but it still needs to operate at various power levels under circumstances. Therefore, in developing new hybrid system, it is important to demonstrate its capability to cover various power levels. In the following sections, we firstly introduce the hybrid system with optimally-downsized engine based on the analyses from Section 3 (Section 4.1), and the strategy for power variation of the newly-developed system (Section 4.2) and the system performance (Section 4.3) are discussed.

4.1 Optimized MCFC-HCCI engine hybrid system

In Section 3, the two methods for downsizing the HCCI engine, i.e. the use of turbocharger and high geometric compression ratio, were discussed. In this section, the new hybrid system is developed by combining these two strategies. In this way, the bottoming cycle of the hybrid system is now composed of a turbocharger and a HCCI engine with higher geometric compression ratio. In Section 3, the turbocharger was analyzed under various compressor pressure ratios, from 1.25 to 2.5, and the geometric compression ratio of the HCCI engine was varied between 12.5

and 22.5. Although both higher compressor pressure ratio and geometric compression ratio can be combined to maximize the downsizing ratio, there is a possibility that the engine may suffer mechanical issues in a real-world application. For this reason, we decided that the pressure ratio of the turbocharger is 1.5 and the geometric compression ratio of the engine is 15. The downsized engine specification is listed in Table 4.1. The engine volume is only ~40% level of the one in the previous hybrid system. The operating conditions and the stream properties for the hybrid system at design-point operation are shown in Table 4.2 and 4.3 respectively. By integrating the turbocharger, there are additional states to be noted. The air-fuel mixture (state 6a) enters the compressor at 1 bar, 58°C, and then the mixture (state 7) exits the compressor at 1.5 bar, 107°C. The engine exhaust gas (state 8a) at 1.59 bar and 610°C, which enters the turbine, expands to the atmosphere pressure gas (state 9) at 1 bar and 561°C. The system performance data at the design point will be discussed with those of the other power levels in Section 4.3.

4.2. Operating strategy for power variation

In this section, the optimized hybrid system developed in Section 4.1 is analyzed at off-design operations with various fuel cell power output levels. A part-load operation for both standalone and hybrid fuel cell systems has been studied by several researches [5, 11, 12, 21]. Liu et al.

studied MCFC and micro-gas turbine hybrid system at part-load operation by using different control methods , which are varying fuel, changing speed of gas turbine and using air-bypass model [5]. Sanchez et al. showed MCFC-Stirling engine hybrid system operation at part-load by controlling the fuel mass flow and utilization factor [11]. Escalona et al. also analyzed hybrid systems at part-load operation. Bottoming cycle of their hybrid systems is configured by SCO2 turbine or Stirling engine. By using some strategies , which are the methods controlling the shaft speed, the hybrid systems are operated under various load range [12]. Marra et al. studied 1 MW MCFC system. They simulated the system for 25-100% load, respectively, and compared the results among these operating conditions [21].

In this study, the MCFC-HCCI engine hybrid system is analyzed at 75-100% fueling levels of the design point to demonstrate a possibility that the hybrid system can be driven under various power output requirements. Here, the percentage of the fueling level is based on the methane flow rate (while keeping the same S/C ratio) into the hybrid system. The reason for choosing the fueling level, instead of power level, as the test parameter is simply for convenience purpose in performing simulation, and it is noted that the power output level is very close to the fueling level due to the similar system efficiency under the tested conditions. Since the proposed hybrid system has two independently

operating components coupled together, it requires systematic control strategies for off-design operation. Firstly, fuels (methane and steam, state 1) are reduced to the desired fueling level, while keeping the same fuel utilization at 70% in the MCFC stack. Secondly, air entering the cathode of MCFC is also reduced following the decreased fueling rate. However, the decreasing proportion is not exactly the same as that of the fueling rate, because the air utilization factor is changed. At design point operation, the air utilization factor is kept near ~40%. The reason of this choice is to reduce the concentration overvoltage at the end of the cathode channels by leaving the sufficient concentration of oxygen, and to prevent the excessive temperature rise in the MCFC by carrying heat out with the extra air flow. However, as shown in Fig. 4.2, the air utilization needs to be increased as the power level is reduced. This is purely the outcome of the system configuration and constraints we apply to. Since the fueling rate is reduced at the lower power operation, the mass flow rate of the anode-off gas is also reduced. To compensate for the reduced flow rate from the fuel cell to the engine, the engine is supplied with more air (state st). Then, the intake charge (state 8) is composed of more air and less anode-off gas than otherwise, which has higher specific heat ratio. In a given geometric compression ratio, this higher specific heat ratio can lead to more temperature increase during the main compression stroke of the engine, which achieves the higher temperature with the

same initial temperature of the mixture. In other words, the intake charge temperature should be reduced to achieve the similar post-compression temperature and thus proper combustion timing for the reduce power level operation. However, the intake temperature reduction also brings in the exhaust temperature decrease. This can cause the possibility of not being able to meet the cathode inlet (state 13) temperature requirement of ~580°C. Therefore, the effectiveness of HX3 should be increased to preheat the cathode air to higher temperature level, but there is the constraint of the maximum effectiveness of 85%. Accordingly, we resolved this conflict by applying two methods. The one isreducing the cathode air flow rate (state 11) more rapidly than the fueling rate decrease and allowing higher air utilization in the fuel cell operation. Still, we are enforcing the maximum temperature rise through the fuel cell less than 100 degrees for the longevity of the fuel cell stack, which sets the highest air utilization or the most reduction of the cathode air flow that we can exploit. Thus, below certain fueling level variation, the engine intake charge temperature can't be reduced to the point where the post-compression temperature achieves similar level as at the design point. Accordingly, the other method, which is rising the engine intake charge temperature, is adopted. And the technique results in slightly higher post-compression temperature and thus earlier combustion timings. Figure 4.2 shows the variation of air utilization factors. At the fueling

ratio of 75%, the air utilization is increased up to 55%. Even at this high utilization value, the temperature rise in the MCFC is kept almost at the similar level as at design point, as we intended to. As shown in Fig. 4.3, the combustion timing advances with lower fueling level for the reasons described above. Finally, Fig. 4.4 illustrates the strategy for power variation by controlling various fuel and air flow rates into the hybrid system.

4.3. System performances

As the fueling level decreases, net power output of the system also decreases almost in the same proportion. The overall system efficiency, however, is almost same, as shown in Fig. 4.5. Table 4.4 lists the detailed performance values of MCFC and HCCI engine. When the power output requirement is lower, MCFC operates at lower current density. Then, the various fuel cell losses are also reduced, which leads to overall higher efficiency from the MCFC operation. For the engine efficiency, there are two competing factors to be considered. As mentioned in Section 4.2, the intake charge entering the engine is composed of more air and less anode off-gas at reduced power levels, and thus the specific heat ratio of the charge increases. Generally, higher specific heat ratio leads to higher engine efficiency. However, the combustion timings, as shown in Fig. 4.3, were advanced at lower power levels, which exacerbated the heat transfer

amount with earlier combustion timings and thus lowered the engine efficiency. As can be seen in Table 4.4, the engine efficiency decreases with lower power output levels, which imply that the second factor has more influence than the first. Finally, combining both MCFC and engine output results in overall similar efficiency values, although the power level is changed.

Table 4.1 Engine geometry and operating conditions

Bore (mm)	121
Stroke (mm)	121
Cylinders	8
Displacement (L)	7.42
Pressure ratio	1.5
Compression ratio	15
Engine speed (rpm)	1800
Equivalence ratio	1 (Stoichiometric)

Table 4.2 System operating conditions at design point

LHV CH_4(kW)	500
Fuel utilization factor (%)	70
Air utilization factor (%)	40
S/C ratio (H_2O:CH_4)	2.5 : 1

Table 4.3 Stream properties for hybrid system at design point

				Mass Concentration (%)							
State	T (°C)	P (bar)	m_{dot} ($kg \cdot s^{-1}$)	Ar	CH_4	CO	CO_2	H_2	H_2O	N_2	O_2
1	30	1	0.0381	-	26.3	-	-	-	73.7	-	-
1a	280	1	0.0381	-	26.3	-	-	-	73.7	-	-
2	570	1	0.0381	-	26.3	-	-	-	73.7	-	-
3	658	1	0.1524	-	-	3.82	67.0	0.50	28.7	-	-
4	541	1	0.1524	-	-	3.82	67.0	0.50	28.7	-	-
5	110	1	0.1524	-	-	3.82	67.0	0.50	28.7	-	-
5a	65	1	0.1524	-	-	3.82	67.0	0.50	28.7	-	-
6	65	1	0.1324	-	-	4.40	77.1	0.58	17.9	-	-
6a	58	1	0.1324	-	-	3.37	59.1	0.44	13.7	17.9	5.45
7	107	1.50	0.1728	-	-	3.37	59.1	0.44	13.7	17.9	5.45
8	301	1.50	0.1728	-	-	3.37	59.1	0.44	13.7	17.9	5.45
8a	610	1.59	0.1728	-	-	3.37	59.1	0.44	13.7	17.9	5.45
9	561	1	0.1728	-	-	0.05	64.3	-	17.7	17.9	0.04
10	30	1	0.3271	-	-	-	-	-	-	76.7	23.3
11	305	1	0.3271	-	-	-	-	-	-	76.7	23.3
12	595	1	0.3271	-	-	-	-	-	-	76.7	23.3
13	582	1	0.4999	-	-	-	22.2	-	6.11	56.4	15.3
14	658	1	0.3856	-	-	-	7.08	-	7.92	73.1	11.9
15	436	1	0.3856	-	-	-	7.08	-	7.92	73.1	11.9
15a	391	1	0.3856	-	-	-	7.08	-	7.92	73.1	11.9
16	278	1	0.3856	-	-	-	7.08	-	7.92	73.1	11.9
st	30	1	0.0404	-	-	-		-	-	76.7	23.3

Table 4.4 Hybrid system performances under power variation

Parameter	Hybrid System (100%)	Hybrid System (95%)	Hybrid System (90%)	Hybrid System (85%)	Hybrid System (80%)	Hybrid System (75%)
LHV CH_4(kW)	500	475	450	425	400	375
Utilization factor (%)	70					
Net MCFC Output (kW)	262	249	237	225	214	200
MCFC Efficiency (%)	58.1	58.3	58.5	58.9	59.4	59.5
Engine Output (kW)	53.6	52.4	48.8	44.2	39.9	36.5
Engine Efficiency (%)	35.6	36.4	35.9	34.8	33.9	32.76
Net Power Output (kW)	315	302	286	270	254	237
System Efficiency (%)	63.0	63.5	63.5	63.4	63.4	63.3

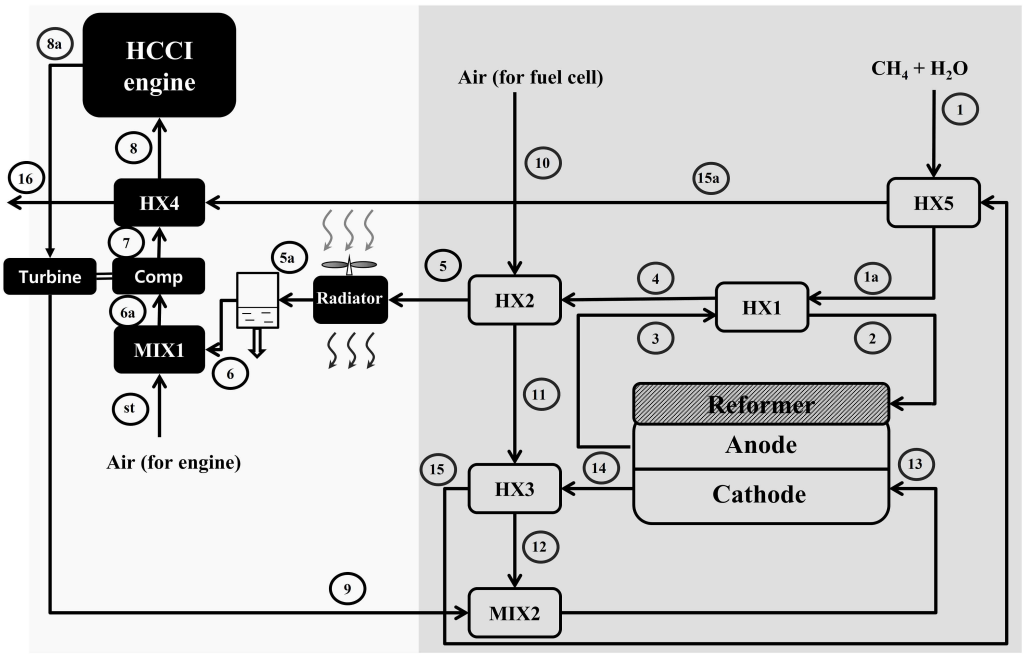

Figure 4.1 New hybrid system configuration (reproduced)

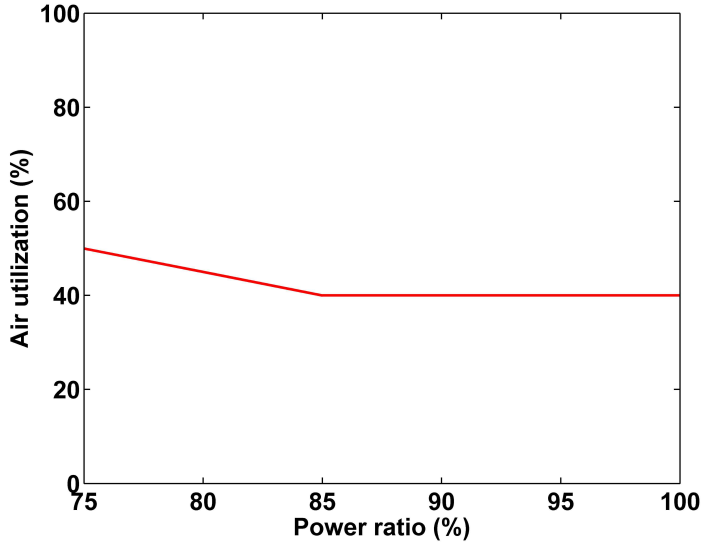

Figure 4.2 Air utilization in MCFC under power variation

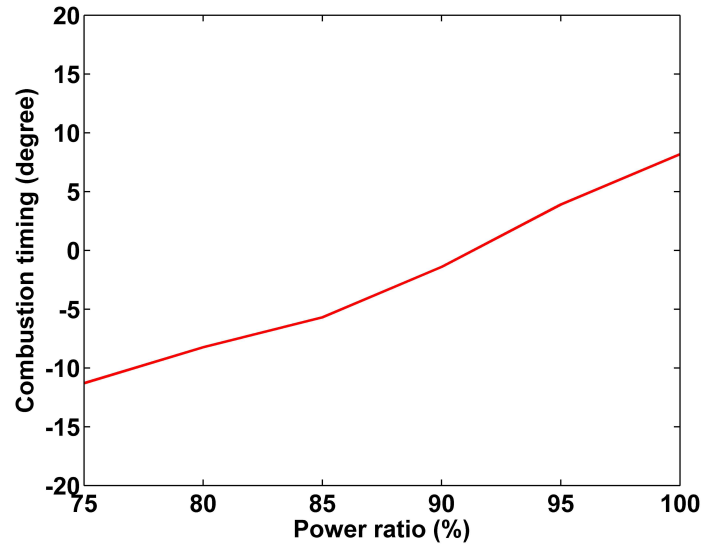

Figure 4.3 Combustion timing in HCCI engine under power variation

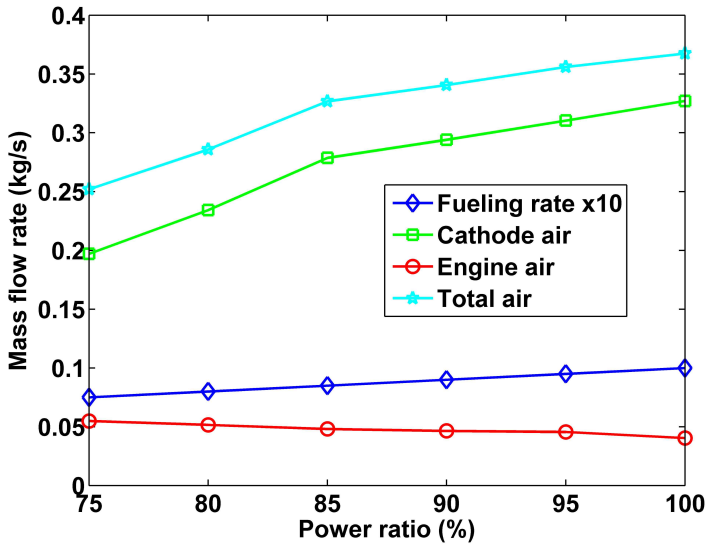

Figure 4.4 System intake mass flow rate under power variation

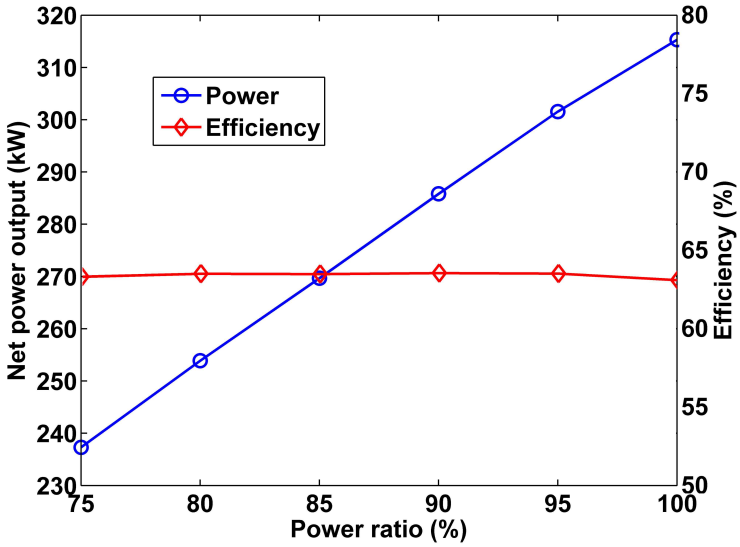

Figure 4.5 Hybrid system power output and efficinecy uner power variation

5. Conclusions

The authors previously developed a new hybrid system of MCFC and HCCI engine, which yields more power output and thus higher efficiency. In this study, improvement in the HCCI engine design in the original hybrid system and development of operating strategies for the power variation were carried out. In the new engine design, we were focusing on the downsizing of the engine to reduce the system cost and increase the specific power output of the engine. Two strategies were suggested, i.e. the use of a turbocharger and the high geometric compression ratio of the engine. To develop the optimized system, the parametric study was performed for various pressure ratios of the turbocharger and for range of geometric compression ratios. Finally, an optimized engine system was chosen for the design-point operation, and in addition, the strategy for off-design operation or part-load operation was developed for it.

The modeling was performed by using the Mathworks MATLAB and Cantera thermo-chemical toolbox. The MCFC stack model, previously developed by the authors was adopted, which also considered non-isothermal behavior as well as internal reforming process. The model calculates the fuel cell losses, temperature change, concentration change, and the fuel cell performance. The HCCI engine model predicts the combustion timing and engine performance by using GRI 3.0 chemical reaction mechanism. The turbocharger model calculates the performances

of the compressor and the turbine. As a result, we can predict a temperature of the compressed gas mixture by the compressor and a temperature of the expanded gas by the turbine.

Here are the summary of the findings:

1. The use of a turbocharger proves itself to be an effective way of engine downsizing. For changing the pressure ratio (PR) of the compressor from 1.25 to 2.5, it is predicted that the engine size can be decreased to the level of 80% at PR of 1.25 and 40% at PR of 2.5, as compared to non-boosting condition. Even with this improvement in engine downsizing, the system power output and efficiency are little affected, in comparison to the performance at design point of the original system.
2. Changing the compression ratio can also be used for engine downsizing, although the effect is relatively limited, as compared to the turbocharger system. At the compression ratio of 12.5, the engine size is 19.2 L, while at 22.5, the engine size is reduced to 16.5 L, which is about 14% reduction. The system power output and efficiency increases a little, mainly due to higher efficiency from the engine operation. At compression ratio of 22.5, the net power output of the hybrid system is 322 kW and the efficiency 64.4%. This corresponds to the 3% increase (relative), as compared to the one with the original engine at the compression ratio of 12.5.

3. To develop the strategy for off-design operation, the new HCCI engine for the hybrid system is chosen as the geometric compression ratio of 15 and with the turbocharger of pressure ratio of 1.5 at design-point operation. This system allows the downsizing the engine by ~60% without significant stress on the mechanical parts of the engine by limiting the peak pressure under 70 bar. With this new design, the system efficiency gains about a 0.5% point. To operate the newly-designed system for varying power levels, fuel flow and air flow rates are adjusted, and the proper heat exchanger operating strategies are suggested. It is demonstrated that the system can run properly at part-load operation (down to ~75% power level of the design point) with the similar system efficiencies.

Appendix A.

In this appendix, MCFC stack modeling is described more detail. The followings are from previous work of authors [13], and referred to the master degree paper of Abid [15]. The present model takes a similar approach as described in Ref. [16] by Baranak et al., although the temperature of the fuel cell is not constant. Some of the governing equations have been reproduced here with subsequent modifications or additions.

The operating unit cell voltage V_{opn} is defined as Eqn. A.1.

$$V_{opn} = E_{rev,i} - \eta_{Nern,i} - j_i R_{total,i} \quad \text{(A.1)}$$

where, for each segment i, $E_{rev,i}$ is the maximum reversible potential, $\eta_{Nern,i}$ is the Nernst loss, j_i is the current density ($A \cdot cm^{-2}$), and $R_{total,i}$ ($\Omega \cdot cm^{-2}$) includes overall irreversible losses in the segment i.

The maximum reversible potential is given by Eqn. A.2.

$$E_{rev,i} = \frac{\Delta G_i}{2f} \quad \text{(A.2)}$$

where △Gi, given by Eqn. A.3, is the Gibbs free energy change per mol of H_2 reacted for segment i, and f is the faraday's constant.

$$\Delta G_i = -24200 + 45.8 T_i \quad \text{(A.3)}$$

where T_i is the isothermal component temperature of each segment i in Kelvin (K).

The Nernst loss for each segment $\eta_{Nern,i}$ is calculated by Eqn. A.4 as

given in Ref. [20].

$$\eta_{Nern,i} = \frac{RT_i}{2f} ln\left[\frac{P_{H_2,and}(P_{O_2,cat})^{\frac{1}{2}} P_{CO_2,cat}}{P_{H_2O,and} P_{CO_2,and}}\right] \qquad \text{(A.4)}$$

where R is the universal gas constant in J/mol-K and P_x is the partial pressure of species x in bars.

$R_{total,i}$ is the sum of all irreversible losses in the segment i and is given by Eqn. A.5.

$$R_{total,i} = R_{and,i} + R_{cat,i} + R_{int,i} \qquad \text{(A.5)}$$

where $R_{and,i}$ and $R_{cat,i}$ are irreversible losses associated with activation energies at anode and cathode, respectively, and $R_{int,i}$ is the ohmic loss associated with resistance in the electrolyte.

The irreversible losses are then calculated by the following empirical relationships, Eqns. A.6-A.8, as given in Ref. [23].

$$R_{and,i} = H_a e^{\Delta H_a / RT_i} P_{H_2}^{-0.5} \qquad \text{(A.6)}$$

$$R_{cat,i} = H_{C1} e^{\Delta H_{C1} / RT_i} P_{O_2,cat}^{-0.75} P_{CO_2,cat}^{0.5} + H_{C2} e^{\Delta H_{C2} / RT_i} M_{CO_2,cat}^{-1.0} \qquad \text{(A.7)}$$

$$R_{int,i} = H_{ir} e^{\Delta H_{ir} / RT_i} \qquad \text{(A.8)}$$

where $M_{CO_2,cat}$ is the mole fraction of CO_2 at cathode, H_x values are apparent frequency factors and ΔH_x values are apparent activation energies in J/mol, both of which are based on Arrhenius plots for Li/Na cells. The values for these parameters are directly adopted from Ref. [23]

and listed in Table A.1.

Rearranging Eqn. A.1, we can obtain the current density by Eqn. A.9.

$$j_i = \frac{E_{rev,i} - V_{opn} - \eta_{Nern,i}}{R_{total,i}} \qquad \text{(A.9)}$$

where V_{opn} is a constant value throughout the unit cell, whereas $E_{rev,i}$, $\eta_{Nern,i}$, $R_{total,i}$ and j_i change from segment to segment. The iterative process to determine the value of V_{opn} is described at Fig.2.4 in Section 2.

Once the current density, j_i is evaluated, the current in each segment can be obtained by Eqn. A.10.

$$i_{seg,i} = j_i A_{seg} \qquad \text{(A.10)}$$

where A_{seg} is the area of each segment, 400 cm^2, which is $1/25^{th}$ of the total cell area i.e. 10,000 cm^2 , which represents a typical unit cell size.

The amount of current generated in each segment is directly related to the consumption of each reactant species, according to Eqns. A.11-A.15.

$$\Delta F_{H_2,and} = -0.018655 i_{seg} \qquad \text{(A.11)}$$

$$\Delta F_{H_2O,and} = -\Delta F_{H_2,and} = 0.018655 i_{seg} \qquad \text{(A.12)}$$

$$\Delta F_{CO_2,and} = -\Delta F_{H_2,and} = 0.018655 i_{seg} \qquad \text{(A.13)}$$

$$\Delta F_{CO_2,cat} = \Delta F_{H_2,and} = -0.018655 i_{seg} \qquad \text{(A.14)}$$

$$\Delta F_{O_2,cat} = \left(\frac{1}{2}\right) \Delta F_{H_2,and} = -0.0093275 i_{seg} \qquad \text{(A.15)}$$

where $\Delta F_{x,cat}$ and $\Delta F_{H_2,and}$ are molar flow rate changes of species x at

cathode and anode, respectively.

After the electrochemical reaction occurs with consequent compositional change in the anode mixture by Eqns. A.11-A.13, it is assumed that the water-gas-shift-reaction occurs very fast to achieve new equilibrium composition. The equilibrium constant (K_P) for this reaction is given by Eqn. A.16.

$$K_P = \frac{P_{CO_2} P_{H_2}}{P_{CO} P_{H_2O}} \qquad \text{(A.16)}$$

Here, the partial pressure of species x is defined by Eqn. A.17.

$$P_x = \frac{F_x}{F_{total}} P_{total} \qquad \text{(A.17)}$$

where P_x and F_x are partial pressure and molar flow rate for species x, respectively. P_{total} is the total pressure and F_{total} is the total molar flow rate.

The relationship between equilibrium constant and temperature (Eqn. A.18) is obtained from Ref. [23].

$$\ln(K_P) = 4276/T_i - 3.961 \qquad \text{(A.18)}$$

To evaluate the compositional change of each reactant by water-gas-shift-reaction, K_P is defined in terms of conversion degree of X and molar flow rate of species, as shown in Eqn. A.19.

$$K_P = \frac{(F_{CO_2} + X)(F_{H_2} + X)}{(F_{CO} - X)(F_{H_2O} - X)} \qquad \text{(A.19)}$$

Rearranging Eqn. A.19, we have an equation for X (Eqn. A.20). By solving it, the conversion degree X is determined.

$$(1-K_P)X^2+[F_{H_2}+F_{CO_2}+K_P(F_{CO}+F_{H_2O})]X+[(F_{CO_2}F_{H_2})-(F_{CO}F_{H_2O})K_P]=0$$

(A.20)

Then, the equilibrium molar flow rates at the anode outlet of the isothermal component of each segment (state 2 in Fig. 2.1) can be evaluated by Eqns. A.21-A.24.

$$F_{H_2,after\ WGSR}=F_{H_2}+X \qquad (A.21)$$

$$F_{CO_2,after\ WGSR}=F_{CO_2}+X \qquad (A.22)$$

$$F_{CO,after\ WGSR}=F_{CO}-X \qquad (A.23)$$

$$F_{H_2O,after\ WGSR}=F_{H_2O}-X \qquad (A.24)$$

The work output from each segment is determined by Eqn. A.25.

$$W_{out,i}=V_{opn}i_{seg,i} \qquad (A.25)$$

Using the enthalpies of the flows entering ($H_{in,i}$) and leaving ($H_{mid,i}$) the isothermal component, $Q_{isothermal,i}$ can be evaluated by Eqn. A.26.

$$Q_{isothermal,i}=H_{in,i}-H_{mid,i}-W_{out,i} \qquad (A.26)$$

where $Q_{isothermal,i}$ is the exothermicity from the electrochemical reaction in a segment i.

Finally, this allows us to calculate the enthalpy of the flow exiting the designated segment i ($H_{out,i}$) after the non-isothermal component by Eqn. A.27.

$$H_{out,i} = H_{mid,i} - Q_{isothermal,i} - Q_{ref,i} \qquad \text{(A.27)}$$

where $Q_{ref,i}$ is $1/25^{th}$ of the total energy required for the reforming process that is distributed uniformly through the segments.

It is assumed that the chemical reactions occur only in the isothermal component, and hence there is no change in composition across the non-isothermal component.[2] Only the exit temperature of a segment is calculated by the outlet enthalpy ($H_{out,i}$) from Eqn. A.27 and the compositions from Eqns. A.14, A.15, A.21-A.24.

After determining the thermodynamic state at each segment exit, the above processes are repeated for the next segment. Once the calculation is completed for 25 segments, the total fuel cell current is evaluated as the sum of the currents from all the segments (Eqn. A.28).

$$i_{unit\,cell} = \sum i_{seg,i} \qquad \text{(A.28)}$$

This corresponds to the current from a single unit cell. To find total current in the fuel cell stack, it is then multiplied by the number of unit cells in a stack.

$$i_{stack} = i_{unit\,cell} \times Nmber\,of\,unit\,cells \qquad \text{(A.29)}$$

where Number of unit cells are assumed to be 250 for this study. Total work output from the fuel cell stack can be determined by Eqn. A.30.

---

2) One may consider re-equilibration of the mixture composition and accompanying temperature change by applying WGSR in the non-isothermal component, but the overall result would change little, if the size of the segment is chosen to be sufficiently small.

$$W_{out} = V_{opn} i_{stack} \qquad \text{(A.30)}$$

To prevent the fuel cell from fuel starvation, a certain level of excess fuel should be supplied, which is quantified as fuel utilization factor (U_f) and the calculation is based on Eqn. A.31.

$$U_f = 1 - \frac{LHV_{an,out}}{LHV_{fuel}} \qquad \text{(A.31)}$$

where $LHV_{an,out}$ is the lower heating value of anode off-gas and LHV_{fuel} is the lower heating value of the original fuel supplied.

Table A.1 Parameters for Irreversible Losses

Parameter	Value
H_{C1}	3.28×10^{-9}
H_{C2}	3.29×10^{-6}
H_a	2.04×10^{-3}
H_{ir}	1.12×10^{-2}
ΔH_{C1} $(j\cdot mol^{-1})$	132,000
ΔH_{C2} $(j\cdot mol^{-1})$	67,100
ΔH_a $(j\cdot mol^{-1})$	23,700
ΔH_{ir} $(j\cdot mol^{-1})$	23,000

Appendix B.

In this appendix, modeling process of an HCCI engine is discussed in detail. The original contents are from the author's previous work [17] and some of the major equations are reproduced here.

The present model assumes a homogeneous thermodynamic state for in-cylinder mixture and only includes compression and power strokes without gas exchange. A series of ODEs are solved for the state variables-crank angle, cylinder volume, temperature, and mass of species-by using an ode solver provided by the Mathworks MATLAB.

The engine is running at a constant speed of n RPM, and the piston location is given by crank angle θ

$$\dot{\theta} = n \qquad \text{(B.1)}$$

The instantaneous cylinder volume (V) is updated by a slider-crank relationship from Heywood [27]

$$\dot{V} = \frac{\pi}{4} B^2 a \dot{\theta} \left(\sin\theta + \frac{a sin\theta \cos\theta}{\sqrt{l^2 - a^2 \sin^2\theta}} \right) \qquad \text{(B.2)}$$

where B is the bore, a is the crank radius, and l is the connecting rod length. The energy equation is solved for the instantaneous cylinder temperature T. Using the first law of thermodynamics for an adiabatic, closed, reacting system it is possible to write

$$\dot{U} = -P\dot{V} \qquad \text{(B.3)}$$

$$mC_v\dot{T}+\sum_i \dot{m}_i u_i + P\dot{V}=0 \qquad \text{(B.4)}$$

$$\rightarrow\ \dot{T}=-\frac{1}{mC_v}\left(\sum_i \dot{m}_i u_i + P\dot{V}\right) \qquad \text{(B.5)}$$

Where U is the total (extensive) internal energy, m is the total mixture mass, C_v is the specific heat at constant volume for the total mixture, m_i and u_i are the mass and internal energy of the ith species, respectively, and P is the instantaneous cylinder pressure. Here, the production (or destruction) rate of species mass m_i by chemical reactions is evaluated by using a function from the Cantera toolbox, which refers to GRI 3.0 mechanisms. Finally, the instantaneous cylinder pressure P is evaluated by using the ideal gas law

$$P=\frac{mRT}{V} \qquad \text{(B.6)}$$

where R is the mass-based gas constant.

References

1. P. Tomczyk, 2006, MCFC versus other fuel cells-Characterisitics, technologies and prospects, J. Power Source, 160, pp.858-862.
2. P. Lunghi, R. Bove, U. Desideri, 2003, Analysis and optimization of hybrid MCFC gas turbines plants, J. Power Source, 118, pp.108-117.
3. R. Roberts, J. Brouwer, E. Liese, R. Gemmen, 2006, Dynamic simulation of carbonate fuel cell-gas turbine hybrid systmes, J. Eng. Gas Turbines Power, 128, pp. 294-301.
4. S. Ubertini, P. Lunghi, 2001, Assessment of an ambient pressure MCFC: External heated GT hybrid plant with steam injection and post-combustion, Fuel Cells, 1.3-4, pp.174-180.
5. A. Liu, Y. Weng, 2010, Performance analysis of a pressurized molten carbonate fuel cell/micro-gas turbine hybrid system, J. Power Source, 195, pp.204-213.
6. R. Rashidi, P. Berg, I. Dincer, 2009, Performance investigation of a combined MCFC system, Int. J. Hydrogen Energy, 34, pp.4395-4405.
7. F. Orecchini, E. Bocci, A. Di Carlo, 2006, MCFC and microturbine power plant simulation, J. Power Sources, 160, pp.835-841.
8. G. Angelino, D. Energetica, P. Paliano, D. Meccanica, 2000, Orgnic rankine cycles (ORCs) for energy recovery from molten carbonate fuel cells, Energy Conversion Engineering Conference and Exhibit 35th

Intersociety, 2, pp. 1400-1409.

9. D. Sanchez, J. M. Escalona, B. Monje, R. Chacartegui, T. Sanchez, 2011, Preliminary analysis of compound systems based on high temperature fuel cell, gas turbine and organic Rankine cycle, J. Power Sources, 196(9), pp.4355-4363.
10. A. Vatani, A. Khazaeli, R. Roshandel, M. Panjeshahi, 2013, Thermodynamic analysis of application of organic Rankine cycle for heat recovery from an integrated DIR-MCFC with pre-reformer, Energy Convers. Manag., 67, pp.197-207.
11. D. Sanchez, R. Chacartegui, M. Torres, T. Sanchez, 2009, Stirling based fuel cell hybrid systems: An alternative for molten carbonate fuel cells, J. Power Sources, 192, pp.84-93.
12. J. Escalona, D. Sanchez, R. Chacartegui, T. Sanchez, 2013, Performance analysis of hybrid systems incorporating high temperature fuel cells and closed cycle heat engines at part-load operation, Int. J. Hydrogen Energy, 38, pp.570-578.
13. S. Kim, A. R. Abid, J. J. Jang, H. H. Song, S. J. Song, K. Y. Ahn, Y. K. Lee, S. G. Kang, 2013, Development of a hybrid system of molten carbonate fuel cell and homogeneous charge compression ignition engine for distributed power generation, J. Fuel Cell Science and Technology, Accepted July 2013, FC-12-1116 (Research Paper)
14. J. Y. Jung, 2013, A start-up strategy of molten carbonate fuel cell and

internal combustion engine hybrid system for distributed power generation , master's thesis, Seoul national university.

15. A. R. Abid, 2012, A novel fuel cell-IC engine hybrid system for distributed power generation, master's thesis, Seoul national university.
16. M. Baranak, H. Atakul, 2007, A basic model for analysis of molten carbonate fuel cell behavior, J. Power Sources, 172, pp. 831-839.
17. H. H. Song, C. F. Edwards, 2009, Understanding chemical effects in low-load-limit extension of homogeneous charge compression ignition engines via recompression reaction, Int. J. Engine Res, 10(4), pp. 231-250.
18. H. H. Song, A. Padmanabhan, N. B. Kaahaaina, C. F. Edwards, 2009, Experimental study of recompression reaction for low-load operation in direct-injection homogeneous charge compression ignition engines with n-heptane and i-octane fuels. Int. J. Engine Res, 10(4), pp. 215-230.
19. http://www.me.berkeley.edu/gri-mech/.
20. P. Moraal, I. Kolmanovsky, 1999, Turbocharger modeling for automotive control applications, SAE transections, 108(3), pp.1324-1338.
21. D. Marra, B. Bosio, 2007, Process analysis of 1MW MCFC plant, Int. J. Hydrogen Energy, 32(7), pp.809-918.
22. K. Kordesch, G. Simader, 1996, Fuel cells and their applications, VCH, New York, pp.111-113.
23. H. Morita, M. Komoda, Y. Mugikura, Y. Izaki, T. Watanabe, Y.

Masuda, T. Matsuyama, 2002, Performance analysis of molten carbonate fuel cell using a Li/Na electrolyte, J. Power Sources, 112, pp.509-518.

24. J. B. Heywwod, 1988, Internal combustion engine fundamentals, Mcgraw-Hill, Columbus.

요약

분산발전용 용융탄산염 연료전지와 HCCI 엔진의 하이브리드 시스템 최적화

서울대학교 대학원
기계항공공학부
김선엽

환경오염과 에너지 고갈 문제가 대두되며 신재생에너지에 대한 수요가 증가하는 추세이다. 이 때 연료전지 시스템은 그 대안으로 적절한 에너지 공급원이다. 이전에 분산발전형 시스템으로 용융탄산염 연료전지와 내연기관인 HCCI 엔진을 결합한 새로운 개념의 하이브리드 시스템이 개발되었었다. 이 시스템은 촉매연소기 대신 HCCI 엔진을 넣어주어 시스템의 효율을 약 62%로 향상시킬 수 있었다. 하지만 엔진에서 나오는 출력에 비해 엔진의 사이즈가 커 비용적인 측면에서 비효율적임을 알 수 있었다. 따라서 이번 연구에서는 우선적으로 이 시스템의 엔진 사이즈를 줄임으로써 시스템을 최적화시킬 것이다. 엔진 사이즈를 줄이는 방법으로는 터보차저를 사용하는 방법과 엔진의 압축비를 높이는 방법 등이 있다. 이러한 방법들을 이용해 엔진 사이즈를 줄인 최적화된 시스템을 제안할 수 있었으며, 이 엔진의 사이즈는 약 60%

이상이 줄었다. 다음으로 이러한 최적화한 시스템의 구동 범위를 넓히기 위한 연구를 진행하였다. 시스템이 70-100% 수준의 파워에서 구동할 수 있는지 분석하였으며, 분석 결과 시스템이 탈설계점에서도 구동 가능하다는 것을 입증할 수 있었다.

주요어: 용융탄산염 연료전지, 예혼합 압축착화 엔진, 터보차저, 하이브리드 시스템, 최적화, 탈설계점 구동
학번: 2011-23328